

On Modeling Tear Breakup Dynamics with a Nematic Lipid Layer

M.J. Taranchuk¹ and R.J. Braun^{1*}

¹Department of Mathematical Sciences, University of Delaware, 210 South College Avenue, Newark, 19716, DE, USA.

*Corresponding author(s). E-mail(s): rjbrown@udel.edu;
Contributing authors: mjgoeken@udel.edu;

Abstract

One of the main roles of the lipid layer (LL) of the tear film (TF) is to help prevent evaporation of the aqueous layer (AL). The LL thickness, composition, and structure all contribute to its barrier function. It is believed that the lipid layer is primarily nonpolar with a layer of polar lipids at the LL/AL interface. There is evidence that the nonpolar region of the LL may have liquid crystalline characteristics. We investigate the structure and function of the LL via a model of the tear film with two layers, using extensional flow of a nematic liquid crystal for the LL and shear-dominated flow of a Newtonian AL. Evaporation is taken into account, and is affected by the LL thickness, internal arrangement of its rod-like molecules, and external conditions. We conduct a detailed parameter study with a focus on the evaporative resistance parameter, the Marangoni number, and primary liquid crystal parameters including the Leslie viscosities and director angle. This new model responds similarly to previous Newtonian models in some respects; however, incorporating internal structure via the orientation of the liquid crystal molecules affects both evaporation and flow. As a result, we see new effects on TF dynamics and breakup.

Keywords: Tear film, Nematic liquid crystal, Lipid layer, Marangoni effect

1 Introduction

With each eye blink, a thin liquid tear film is established that helps protect and nourish the ocular surface, and helps provide a good smooth surface for clear sight. The tear film (TF) is a multi-layer film, and each layer plays a role in TF dynamics

[1]. Despite the importance of the TF, there is still much that is not understood. This paper develops a new model for how the TF may fail, which is often called tear breakup (TBU). The purpose is to better understand the function and structure of the outermost layer of the TF, called the lipid layer (LL). A prime motivation for understanding TF dynamics and TBU is that these phenomena are thought to contribute to the initiation and progression of dry eye disease (DED), which affects millions of people [2, 3]. For comprehensive views of clinical aspects of DED and the tear film see Refs. [4–8]. Reviews related to the tear film include Refs. [1, 9, 10]. In this introduction, we now describe the overall structure of the LL. We then introduce previous work on properties, proceed to mathematical models of the tear film and its dynamics, and finally discuss details of the LL and our goals for this paper.

1.1 Overall structure of the tear film

At the anterior interface with air is an oily LL that retards evaporation [11, 12], and helps to retain a smooth, well-functioning tear film [13]. The LL also contains polar lipids that are surface active and lower the surface tension between the LL and the aqueous layer (AL), which is posterior to the LL [14, 15]. The AL consists mostly of water [16], but it also contains various ions and proteins [11]. At the corneal surface, which is posterior to the AL, there is a region with transmembrane mucins protruding from the epithelial cells of the cornea or conjunctiva. This forest of glycosolated mucins is called the glycocalyx. It is generally agreed that the presence of the healthy hydrophilic glycocalyx prevents the tear film from dewetting the ocular surface [17–19].

The overall thickness of the TF is a few microns [20], while the average thickness of the LL is on the order of tens to 100 nanometers when the eye is open [10, 13, 21–23]; the thickness of the glycocalyx is a few tenths of a micron [19, 24]. The overall structure is reformed on the order of a second after each blink in a healthy tear film [10, 14, 25, 26].

TBU occurs when a thinned region forms in the TF. Clinically, this is defined as the first dark area that is observed in the fluorescent TF following instillation of fluorescein dye [27]. Various mechanisms are thought to cause different types of TBU, or to combine in various ways: evaporation of water from the AL [7, 28, 29], Marangoni-driven tangential flow (from non-uniform polar lipid surface concentrations) [30], or dewetting-driven tangential flow (from uneven ocular surface conditions) [31–33]. Here, we use the phrase tangential flow to mean flow along the eye. The evaporation of water from the AL causes relatively slow thinning [34], while one may expect rapid thinning to be explained by Marangoni-driven tangential flow [30] or dewetting-driven tangential flow. Concentration gradients from surface active polar lipids in the LL induce shear stress at the LL/AL interface and drive outward tangential flow via the Marangoni effect [14, 15]. Dewetting from irregularities in a corneal surface region has been hypothesized to generate outward tangential flow from internal pressure gradients inside the AL due to van der Waals type forces [31, 35, 36]. A related term is full-thickness tear film breakup (full thickness-TBU), which is when the AL has thinned to the point where the LL and glycocalyx touch [29, 37]. It is our belief that the strongest evidence to date regarding mechanisms for TBU are evaporative and Marangoni-driven thinning and their interaction [38, 39]; unambiguous evidence of

van der Waals-driven dewetting is not yet in hand in our opinion [29]. We now discuss studies of these mechanisms in more detail.

The aqueous part of tear fluid is primarily supplied from the lacrimal gland near the temporal canthus (corner) and the excess is drained through the puncta near the nasal canthus [40]. Water lost from the tear film due to evaporation into air is an important process [11, 41, 42]. We believe that this is the primary mechanism by which the osmolarity (essentially, the total concentration of ions on a molar basis) is increased in the tear film [10]. Some water is supplied from the ocular epithelia via osmosis when the osmolarity increases above the isotonic level (the so-called hyperosmolar state) [10, 41, 43–45]. According to the Dry Eye WorkShop (DEWS) reports, the osmolarity is important because it plays an important etiological role in the development of dry eye disease [28]. An accepted view in the DEWS reports is that repeated exposure to sufficient hyperosmolarity in tears, as may occur in TBU, can result in inflammation and ocular surface damage in a vicious cycle that may lead to DED. There is still considerable ongoing research to more fully understand the causes and etiology of DED; some mathematical modeling results discussed in this paper help to quantify the relationship between tear breakup and hyperosmolarity.

1.2 Measurements and properties

Both TF instability and hyperosmolarity are important to study because they are proposed as etiological causes of dry eye disease [6, 7]. An osmolarity difference between the corneal epithelium and AL induces osmotic flow from the cornea to the TF [10, 46]. TF osmolarity may be measured in the inferior meniscus clinically [47]; the healthy range is 296–302 mOsM [47–49]. Dry eye measurements in the same location can reach 316–360 mOsM [48, 50–52] but estimates for the TF over the cornea reach 900 mOsM or higher [10, 46, 53, 54]. High levels of TF osmolarity are associated with pain, inflammation and cellular changes [53, 55, 56]. In support of these potentially high levels of TF osmolarity over the cornea, mathematical models without spatial variation have estimated peak osmolarities up to ten times the isotonic concentration [10, 43]. The modeling work of Peng et al. [46] found that evaporation elevates osmolarity in breakup regions.

TF thinning rates have been measured experimentally or estimated in many studies. A few experimental methods include spectral interferometry [34, 42, 57], an open chamber [58], an evaporimeter [59], and averaging pure water and functioning LL rates over the cornea obtained by heat transfer analysis and thermal imaging [60]. Parameter estimation schemes were developed in Luke et al. [39, 54] for fitting partial differential equation (PDE) models to experimental fluorescent intensity distributions [61]. They found evaporative thinning rates ranging from 36.9 to $-4.91 \mu\text{m}/\text{min}$ (negative indicates thickening) and overall TF thinning rates ranging from 23.5 to $1.85 \mu\text{m}/\text{min}$. These estimates were quite similar to previous experimental spot-thinning rates that did not specifically seek TBU instances [57].

Tiffany and Dart [62] measured values of the viscosity of human meibum (the material expressed from the meibomian glands inside the lids) using a capillary tube and they estimated values from 9.7 to 19.5 Pa s at 308 K. This is a representative value for the temperature on the surface of the tear film [63]. In a series of papers by

Tiffany and coworkers, the human tear film has been shown to have non-Newtonian properties [64–66]. Tiffany [66] found that whole tears, that is, tear sampled directly from the eye, are shear thinning. The shear thinning has been fit with empirical models, namely Cross [66] and Ellis models [67]. Tiffany [64] also found weak elastic effects; Tiffany and Nagyová [68] found that removing all lipids from tears caused tear fluid to become Newtonian. The rheology of the LL depends on temperature [69]; *in vitro* observations showed temperature dependence of meibum on saline for monolayers [70, 71] and for bulk samples [72]. The elastic contributions to viscous response was small above 305 K for these measurements [70]. King-Smith et al. [23] used high-resolution microscopy to observe LL dynamics, and they saw fine structure of the LL during the interblink period that included islands of lipids.

The surface tension of the tear/air interface was measured to be 46.2 mN/m by Miller [73] *in vivo* using a special contact lens; this is about 2/3 that of an air/pure-water interface. Pandit et al. [65] measured the surface tension of whole tears with a capillary tube and obtained 43 mN/m for unstimulated tears and 46 mN/m for stimulated tears; Miller [73] likely measured stimulated tears. A value of 45 mN/m is often used in theoretical studies. The components responsible for lowering the surface tension from that of pure water has been the subject of a number of papers [68, 74–76]. A challenge for this measurement is the dependence of surface tension on surface active components like phospholipids and other lipids [77–79] and still other species [80]. Detailed equations of state for studying the Marangoni effect from these species is not available for the tear film *in vivo* to our knowledge, and this is an ongoing area of research.

1.3 Mathematical modeling

A variety of mathematical models have incorporated various important effects of tear film dynamics as has been recently reviewed [10, 43, 81]. The most common assumptions for these models are a Newtonian tear fluid and a flat cornea [14, 82]. One category of models treats the flow over an open eye-shaped domain; these models have used lubrication theory with two space dimensions and time as independent variables [83–87]. These papers were on a stationary domain, and emphasized the effects of supply and drainage, osmolarity in various locations in the tear film, and the overall appearance of fluorescein imaging of the tear film. Some initial studies have examined flow on a blinking domain [81, 88, 89], but they have yet to incorporate the same level of effects as in the static boundary papers. There have also been useful compartment models developed for tear film dynamics [44, 90]. These models use compartments of the tear film as dependent variables in systems of ordinary differential equations (ODE) and thus avoid the computational difficulties of solving PDEs on 2D domains. The models can be solved over many blinks and give insight into the osmolarity and other variables at various operating conditions.

There are quite a few models that have been developed using a single variable in space and time for independent variables. There are two main categories here: (1) a spatial domain that extends across the eye opening vertically, with or without a moving end, and (2) a shorter domain that is a local model for TF dynamics. We first discuss category (1). First, a number of papers considered a domain that

extended across the open eye with fixed ends which typically called post-blink drainage models [91–94]. These models typically imposed large menisci at the domain ends that drained fluid from the relatively flat interior of the TF, and that drove the dynamics. Notable among these papers is that evaporation was included to find that it could drive thinning to TBU [94], and that a moving end, representing the upstroke of the blink, was treated as a coating flow problem [92]. Both of those aspects would find many applications in later papers. Heat transfer and evaporation were considered in Li and Braun [95], and later treated together with thermal imaging in Dursch et al. [60]. A counterpoint to these papers Berger and Corrsin’s treatment of the Marangoni effect in post blink spreading [14], which provided a basis for using this effect in many later papers.

Using a moving end on a one-dimensional domain to simulate the upper eyelid during a blink has been employed in a number of papers. The first to do this was by Wong et al. [92]; they treated the problem as a coating flow analysis and developed a closed form equation for the thickness of the deposited film as a function of end (lid) speed. Later papers extended this analysis by computing the thickness and other TF variables numerically. These included a combined TF formation and drainage model [96], and then adding surfactant transport on the surface of the TF [97]. Additional papers using the eye opening and interblink together included gravity and reflex tearing [98]; using optimization varying viscosity to simulate and design eyedrops [67]; a detailed look at insoluble surfactant [99]; a (Newtonian) two-layer model of the tear film with insoluble surfactant between them [100]; the effect of (constant) globe curvature on tear film thickness [101]; and a shear-thinning (power law) model for TF thickness on a curved substrate [102]. Some papers also treated the moving end for complete blink cycles. Simple sinusoidal motion was treated in Braun and King-Smith [103], while more realistic motion was treated in Heryudono et al. [104], and insoluble surfactant was added in Zubkov et al. [105]. Heat transfer was later considered with either full [106] or partial [107] blink cycles.

We next discuss category (2) which are local one-dimensional models for TF dynamics. These models are along a short line segment and are designed to be local models of TF flow. The effects of evaporation and the Marangoni effect on TBU have been studied in a number of papers. Evaporation drove all the dynamics in the models in [10, 46, 61], though the treatments were different. In [46], a stationary LL with variable thickness caused increased localized thinning; also included were osmolarity transport in the AL and osmosis across the AL/cornea interface. An important result from that work is that diffusion of osmolarity out of the region of evaporation prevents osmosis from stopping thinning as it would in spatially uniform models [10, 43]. Simpler evaporation models were used in [10, 61], but they included transport of fluorescein so that they could explain what was seen in TF visualization experiments. Zhong et al. [30] developed a PDE model with one spatial variable that incorporated both mechanisms. Including fluorescein dye transport and fluorescence enabled fitting of models to *in vivo* fluorescence data within TBU regions to estimate parameters that are not possible to directly measure there at the time of writing [39, 54]. Recently, ODE models with no space dependence have been successfully fit to fluorescence data

in small TBU spots and streaks [108]. Those models have been coupled to a neural-network based data extraction system to greatly expand the amount of TBU instances that may be studied [109].

Other effects have been included in local models of TBU [30–32, 46, 61, 110–114]. Some models incorporated the effect of soluble mucins in the AL necessitating departure from more standard lubrication models [112, 113]. Localized non-wettability of the ocular surface was modeled in [114]. Other models have provided fundamental analyses on evaporation [115, 116] and instability [117, 118].

1.4 LL structure and the model in this paper

The composition and structure of the LL, and their relation to function, are the subject of much ongoing research [77, 119, 120]. The complexity of the composition affects the determination of structure and function, and has led to a variety of perspectives in this area [80, 121]. It is generally thought that the LL has an outermost nonpolar LL with a layer of polar lipids and other surface active components at the LL/AL interface [1, 122]. Measuring all but the most basic properties can be a challenge, however. Microscopy has shown some example forms that the LL may take [23]; the shapes observed there suggest non-Newtonian behavior of the LL [71, 72]. For a number of years, it was very difficult to reproduce significant resistance to evaporation using *in vitro* meibum or LL films [123, 124], even though resistance to evaporation has been thought to be an important property *in vivo* [11, 34]. However, recent progress on *in vitro* films with many components has been made [12, 125]. The barrier function does depend on thickness [34, 126], but clearly there is an effect from internal structure as well [127, 128].

Molecular dynamics simulations, together with Langmuir trough experiments, have also given insight into the structure and function of the LL or model systems for it. Coarse grained models were initially employed [129, 130] and those models suggest that the LL may not be so well organized as layers of nonpolar lipids atop a polar lipid monolayer. Later, all-atom models have suggested that the specific polar lipids [131, 132] and wax esters [133] may form ordered states to slow evaporation of water from the AL. Molecular dynamics simulations are likely to continue to give important insights into LL structure and function, but they currently can only be solved at small space and time scales. A link to bigger scales has been made via Langmuir trough observations with Brewster angle microscopy, e.g. [131, 132] for equilibrium states. Those insights need to be converted to larger scale dynamic models to address other situations such as TBU. In this paper, we develop a two-layer continuum model that attempts to incorporate some internal structure of the LL that may be expected to produce evaporation resistance [29, 38] that depends on that structure. We use a nematic liquid crystal structure as a model for the LL, which can show birefringence as has been observed for meibum [134].

Adapting two-layer models of tear dynamics [46, 100] to dynamic models of local TBU regions [135, 136] has made use of extensional flow for the LL and shear dominated flow for the AL. These models have a common basis from the approach of Matar et al. [137]. Of particular interest here is including extensional flow of a nematic liquid crystal [138, 139] for the LL with a Newtonian shear-dominated AL

We model the AL using the Navier-Stokes equations, and the LL using the Ericksen-Leslie equations for nematic liquid crystals. We use the following scalings, where primes denote dimensional quantities. The coordinates (x', y') and velocity components (u'_i, v'_i) correspond to the axial and transverse directions respectively, t' is time, and p'_i is pressure. The subscript i indicates the fluid layer under consideration; $i = 1$ corresponds to the AL, and $i = 2$ corresponds to the LL.

$$\begin{aligned}
x' &= Lx, & h'_1 &= \epsilon L h_1, & h'_2 &= \epsilon \delta L h_2, \\
y' &= \epsilon L y, & u'_1 &= U u_1, & u'_2 &= U u_2, \\
h' &= \epsilon L h, & v'_1 &= \epsilon U v_1, & v'_2 &= \epsilon U v_2, \\
t' &= \frac{L}{U} t, & p'_1 &= \frac{\mu_1 U}{\epsilon^2 L} p_1, & p'_2 &= \frac{\mu_2 U}{L} p_2, \\
\Gamma' &= \Gamma_0 \Gamma, & c' &= C c, \\
J'_o &= \epsilon U J_o, & J'_e &= \epsilon \rho_1 U J_e.
\end{aligned} \tag{1}$$

Here the total thickness of the tear film $h' = h'_1 + h'_2 \implies h = h_1 + \delta h_2$. The scalings used in the model, chosen with the dimension of the human eye in mind, are defined in Table 1. The LL is the thinnest layer in the tear film, and has an average thickness of tens to 100 nm during the interblink [13, 140–142]. The AL is much thicker, averaging about 3 μm [143]. The glycocalyx is less than a micron thick [19, 24]; while it does not appear in the model explicitly, we account for its height by defining TBU as an AL thickness of 0.5 μm or less. We consider a domain of length 2 mm.

Table 1 Parameters used in dependent variable scalings

Parameter	Value	Units	Description	Reference
$L = H_1(\gamma_1 + \gamma_2)/(\mu_1 E_0)^{1/4}$	3.1779×10^{-4}	m	Length scale	[135]
H_1	3.5×10^{-6}	m	AL thickness	[143]
H_2	5×10^{-8}	m	LL thickness	[140]
$V = E_0$	5.093×10^{-7}	m/s	Thinning rate	[135]
$U = V/\epsilon$	4.624×10^{-5}	m/s	Horizontal velocity	[135]
C	300	mOsM	Reference osmolarity	[46]
Γ_0	4×10^{-7}	mol/m ²	Surfactant concentration	[99, 100]

The nondimensional quantities that result from scalings are given in Table 2, and the physical parameters are listed in Table 3. We note that while experiments show evidence of liquid crystal structure in the LL of the TF, the parameter values for the LL have not been measured. For liquid crystals, we return to a Newtonian fluid by setting the Leslie viscosities $\alpha'_i = 0$, $i = 1, \dots, 6$, $i \neq 4$, and $\alpha'_4 = 2\mu_2$. The dynamic viscosity of the LL, μ_2 , has previously been taken to be 0.1 Pa s [100, 135]. Thus, to match this viscosity in the Newtonian limit, as default values we choose our Leslie viscosities to be three times the properties of 5CB, a liquid crystal that has been relatively well studied near physiological temperatures [144]. We explore a larger range of values in Section 3.1.3.

Table 2 Nondimensional Parameters

Parameter	Formula	Value	Description
ϵ	H_1/L	0.0110	Aspect ratio of AL
δ	H_2/H_1	0.0143	Lipid to aqueous thickness ratio
Υ	$\epsilon^2\mu_2/\mu_1$	0.0091	Reduced viscosity ratio
\mathcal{C}_1	$\epsilon^3(\gamma_1 + \gamma_2)/(\mu_1 U)$	1.0001	Reduced aqueous capillary number
\mathcal{C}_2	$\epsilon\gamma_2/(\mu_2 U)$	43.8371	Reduced lipid capillary number
\mathcal{M}	$\epsilon RT_0\Gamma_0/(\mu_1 U)$	187.7687	Reduced Marangoni number
\mathcal{E}	$E_0/(\epsilon\rho_1 U)$	1.0001	Evaporation parameter
\mathcal{R}_0	$k_m H_2/(Dk)$	17.68	Evaporative resistance parameter
\mathcal{P}	$CP_c/(\epsilon U)$	0.1355	Osmosis parameter
Pe_1	UL/D_1	9.1842	Péclet number for osmolarity diffusion
Pe_s	UL/D_s	0.4898	Péclet number for surfactant diffusion

Table 3 Physical Parameters

Constant	Value	Units	Description	Reference
ρ_1	1000	kg/m ³	Density of liquid water	[145]
ρ_2	900	kg/m ³	Density of lipid	[100]
μ_1	1.3×10^{-3}	Pa s	Dynamic viscosity of water	[66, 100]
$\mu_2 = \alpha'_4/2$	0.0978	Pa s	Dynamic viscosity of lipid	[144]
γ_1	0.027	N/m	Surface tension of water	[146]
γ_2	0.018	N/m	Surface tension of lipid	[147]
R	8.3145	J/(K mol)	Ideal gas constant	[145]
D_1	1.6×10^{-9}	m ² /s	Osmolarity diffusion constant	[148]
D_s	3×10^{-8}	m ² /s	Surfactant diffusion constant	[100]
k_m	0.0182	m/s	Mass transfer coefficient	[135]
Dk	5.136×10^{-11}	m ² /s	Lipid permeability	[135]
P_c	2.3×10^{-10}	kg/(mOsM m ² s)	Corneal osmosis coefficient	[46]
E_0	5.0928×10^{-7}	m/s	Evaporative thinning rate	[135]
T_0	308.15	K	Eye surface temperature	[46]
α'_1	-0.0180	Pa s	Leslie viscosity	[144]
α'_2	-0.2436	Pa s	Leslie viscosity	[144]
α'_3	-0.0108	Pa s	Leslie viscosity	[144]
α'_4	0.1956	Pa s	Leslie viscosity	[144]
α'_5	0.1920	Pa s	Leslie viscosity	[144]
α'_6	-0.0624	Pa s	Leslie viscosity	[144]
θ_B	$0 - \pi/2$	radians	Director angle	[144]

2.1 Governing equations

After nondimensionalizing, we asymptotically expand all of the dependent variables in powers of the small parameter ϵ . We then collect like powers of ϵ , and solve to find a closed system of leading order equations. In the process, we find that the director angle is constant at leading order, $\theta = \theta_B$. We also determine the leading order AL pressure p_1 , and the AL depth averaged axial velocity \bar{u}_1 . This process is described in more detail in the appendix A, and derived thoroughly in Taranchuk and Braun [136]. We find the closed leading order system to be

$$h_{10t} + (\bar{u}_{10}h_{10})_x = J_o - J_e, \quad (2)$$

$$h_{20t} + (u_{20}h_{20})_x = 0, \quad (3)$$

$$-\frac{A(\theta_B)}{B(\theta_B)}\delta\Upsilon(u_{20x}h_{20})_x - \frac{u_{20}}{h_{10}} = \frac{h_{10}}{2} \left(-\mathcal{C}_1 h_{10xxx} - \mathcal{C}_2 \Upsilon h_{0xxx} \right) - \mathcal{C}_2 \delta\Upsilon h_{20} h_{0xxx} + \mathcal{M}\Gamma_{0x}, \quad (4)$$

$$\Gamma_{0t} + (\Gamma_0 u_{20})_x = \frac{1}{Pe_s} \Gamma_{0xx}, \quad (5)$$

$$(c_0 h_{10})_t = \frac{1}{Pe_1} (c_{0x} h_{10})_x - (c_0 \bar{u}_{10} h_{10})_x, \quad (6)$$

where

$$h_0 = h_{10} + \delta h_{20}, \quad (7)$$

$$J_o = \mathcal{P} \left(c - \frac{c_0}{C} \right), \quad (8)$$

$$J_e = \frac{\mathcal{E}}{1 + \mathcal{R}(\theta_B) h_{20}}, \quad (9)$$

$$\mathcal{R}(\theta_B) = \mathcal{R}_0 (0.1 + 0.9 \sin \theta_B), \quad (10)$$

$$p_{10} = -\Upsilon \mathcal{C}_2 h_{0xx} - \mathcal{C}_1 h_{10xx}, \quad (11)$$

$$\bar{u}_{10} = -p_{10x} \frac{h_{10}^2}{12} + \frac{u_{20}}{2}, \quad (12)$$

and

$$\begin{aligned} A(\theta_B) &= 2 \cos(2\theta_B) (\alpha_1 + \alpha_5 + \alpha_6 + 4) (\alpha_2 + \alpha_3 - \alpha_5 + \alpha_6) \\ &\quad + \cos(4\theta_B) (\alpha_1 [\alpha_2 - \alpha_3] + [\alpha_2 + \alpha_3] [\alpha_5 - \alpha_6]) + \alpha_1 \alpha_2 - \alpha_1 \alpha_3 - 2\alpha_1 \alpha_5 \\ &\quad - 2\alpha_1 \alpha_6 - 8\alpha_1 + \alpha_2 \alpha_5 + 3\alpha_2 \alpha_6 + 8\alpha_2 - 3\alpha_3 \alpha_5 - \alpha_3 \alpha_6 - 8\alpha_3 - 2\alpha_5^2 \\ &\quad - 4\alpha_5 \alpha_6 - 16\alpha_5 - 2\alpha_6^2 - 16\alpha_6 - 32, \end{aligned} \quad (13)$$

$$\begin{aligned} B(\theta_B) &= -\alpha_1 \cos(4\theta_B) + \alpha_1 - 2 \cos(2\theta_B) (\alpha_2 + \alpha_3 - \alpha_5 + \alpha_6) \\ &\quad - 2\alpha_2 + 2\alpha_3 + 2\alpha_5 + 2\alpha_6 + 8. \end{aligned} \quad (14)$$

Equation (2) and (3) represent conservation of mass (of solvent) in the AL and LL, respectively. Equation (4) is the axial force balance in the LL. Equation (5) conserves mass of surfactant, and Equation (6) conserves osmolarity in the AL.

The evaporation function in Equation (9) depends on the evaporative resistance in the LL which is described by Equation (10). We vary the evaporative resistance function $\mathcal{R}(\theta_B)$ by changing both \mathcal{R}_0 and θ_B . Various director angles are considered throughout the paper, and Sections 3.1.2 and 3.2.2 focus on the effect of \mathcal{R}_0 for two sets of initial conditions.

2.2 Initial and boundary conditions

2.2.1 Evaporation-driven flow

To illustrate flow driven by evaporation, we choose initial conditions in such way that valley, or thin spot, in the LL drives all the dynamics of the tear film toward TBU. We choose a Gaussian perturbation of the LL

$$h_2(x, 0) = 1 - 0.9e^{-x^2/(2\sigma^2)}, \quad (15)$$

where $2\sigma^2 = 1/9$. We take $h_1 = \Gamma = c = 1$ initially. We compute $p_1(x, 0)$ from Equation (21), and solve the discrete version of the axial force balance Equation (22) using the other initial values to obtain $u_2(x, y, 0)$. This initial condition corresponds to the Gaussian disturbance described in Stapf et al. [135]; we refer to it as a valley here.

2.2.2 Marangoni effect

To illustrate surfactant gradient driven flow, we choose initial conditions in which all variables are uniform initially ($h_1 = h_2 = c = 1$), except for a local excess of surfactant in the center of the domain. We compute $p_1(x, 0) = 0$ and $u_2(x, y, 0)$ as described above. The initial condition for Γ is

$$\Gamma(x, 0) = 1 + s - s \left(\frac{1 + 0.5 \tanh\left(\frac{x-x_0}{x_w}\right) + 0.5 \tanh\left(\frac{-x-x_0}{x_w}\right)}{n} \right) \quad (16)$$

where the height of the region of excess surfactant is $s = 1.8$, the inflection point is $x_0 = 1$, and the width of the region is $x_w = 0.36$, and normalization factor $n = 0.9915$.

2.2.3 Combining LL and surfactant perturbations

Having considered perturbations in the LL and surfactant surface concentration individually, we now consider two scenarios which combine perturbations in both. Namely, we consider a bump in h_2 combined with a local excess of Γ , and a valley in h_2 combined with a local excess of Γ .

Imaging of the LL has shown instances of regions of thicker lipid [22]. It is reasonable to assume that when the LL is thicker, there is more surfactant. To illustrate this, we consider a thin LL with a central bump and central increased Γ in that area. We take $h_1(x, 0) = c(x, 0) = 1$, and we calculate $p_1(x, 0)$ and $u_2(x, 0)$. The initial condition for surfactant is Equation (16), and for LL thickness

$$h_2(x, 0) = 1 + s - s \left(\frac{1 + 0.5 \tanh\left(\frac{x-x_0}{x_w}\right) + 0.5 \tanh\left(\frac{-x-x_0}{x_w}\right)}{n} \right) \quad (17)$$

where the height of the bump is $s = 1$, the inflection point is $x_0 = 1$, and the width of the bump is $x_w = 0.36$, and normalization factor $n = 0.9915$. This corresponds

dimensionally to a LL with background thickness of 25 nm, and a bump of lipid of height 50 nm in the center of the domain.

We also consider a pathological scenario in which a valley in the LL is combined with a local excess of Γ . Keeping all other initial conditions as described above, we modify only Equation (17) by changing $s = -0.5$, creating a valley in the LL. This corresponds dimensionally to a LL with thickness 50 nm, and a valley of depth 25 nm in the center of the domain.

2.2.4 Boundary conditions

At both boundaries we impose the following no flux boundary conditions,

$$h_{1x} = h_{2x} = p_{1x} = \Gamma_x = c_x = 0, \quad (18)$$

and specify $u_2 = 0$ for the LL velocity.

2.3 Numerical solution

Before solving numerically, we make two change of variables. In order reduce the order of the system, we define p_{10} as a dependent variable (Equation (21)) and substitute into Equation (4). We also use the substitution $m_0 = h_{10}c_0$ in Equation (6), where m_0 is the mass. This yields the following closed system which we wish to solve

$$h_{10t} + (\bar{u}_{10}h_{10})_x = J_o - J_e, \quad (19)$$

$$h_{20t} + (u_{20}h_{20})_x = 0, \quad (20)$$

$$p_{10} = -\Upsilon\mathcal{C}_2h_{0xx} - \mathcal{C}_1h_{10xx}, \quad (21)$$

$$-\frac{A(\theta_B)}{B(\theta_B)}\delta\Upsilon(u_{20x}h_{20})_x - \frac{u_{20}}{h_{10}} = \frac{h_{10}}{2}p_{10x} - \mathcal{C}_2\delta\Upsilon h_{20}h_{0xxx} + \mathcal{M}\Gamma_{0x}, \quad (22)$$

$$\Gamma_{0t} + (\Gamma_0u_{20})_x = \frac{1}{\text{Pe}_s}\Gamma_{0xx}, \quad (23)$$

$$m_{0t} = \frac{1}{\text{Pe}_1} \left(m_{0x} - \frac{m_0 h_{10x}}{h_{10}} \right)_x - (m_0 \bar{u}_{10})_x, \quad (24)$$

where

$$h_0 = h_{10} + \delta h_{20}, \quad (25)$$

$$J_0 = \mathcal{P} \left(\frac{m_0}{h_{10}} - 1 \right), \quad (26)$$

$$J_e = \frac{\mathcal{E}}{1 + \mathcal{R}(\theta_B)h_{20}}, \quad (27)$$

$$\bar{u}_{10} = -p_{10x} \frac{h_{10}^2}{12} + \frac{u_{20}}{2}. \quad (28)$$

We then use the method of lines to solve the system numerically subject to the initial and boundary conditions of Section 2.2. Spatial derivatives are approximated

with second-order finite differences on a uniform grid of 512 points. This results in a system of differential algebraic equations that we solve forward in time in MATLAB (MathWorks, Natick, MA, USA) using `ode15s`. We found that the solutions were converged using this number of grid points, and that the mass of water and osmolarity were conserved to the tolerances of the computation.

We integrate the system until either of the following happens: (i) a final time for 60 s is reached, or (ii) TBU occurs. We define TBU as the point at which the AL thickness reaches a minimum value of $0.5\mu\text{m}$, and use event detection to stop the simulation if this happens. When breakup occurs, the TBUT becomes the final time.

3 Results

3.1 Evaporation-driven thinning

As an example of evaporation-driven thinning, we consider the initial conditions described in Section 2.2.1 with a director angle of $\theta_B = 0$. This choice maximizes the evaporation rate for our chosen evaporation function. Evaporative resistance in the LL is maximized for $\mathcal{R}(\pi/2)$; $\mathcal{R}(0)$ reduces that resistance by a factor of 10.

Solutions are shown in Figure 2. The LL changes very little over time, maintaining its original shape with a valley in the center of the domain. The initial velocity in the LL, which ranges between $\pm 50\mu\text{m}$, is moderate compared to the dynamics of other scenarios considered later. The thinning in the LL leads to increased evaporation of the AL, which quickly thins, reaching breakup conditions in the center of the domain by 15.9 s. AL pressure begins to drop in the center of the domain; in general, this would help to restore fluid to the area; however TBU occurs because that capillarity-driven contribution is too weak.

Osmolarity c increases over time, peaking in the center of the domain as a result of increased evaporation in that area. By the final time, osmolarity in the center of the domain is 1651 mOsM, more than five times the initial value; and near the ends it is 789 mOsM, over two and a half times the the initial value.

The surface surfactant concentration Γ , shown relative to its initial value, builds up slightly in the center of the domain. We explore Marangoni-driven flow in detail in Section 3.2; however in this example, the increase in surfactant concentration is not large enough to contribute significantly to the flow.

These solutions are representative of evaporation-driven thinning that leads to breakup before the final time of 60 s. With a larger director angle, evaporation resistance of the LL is increased, and the AL thins more slowly. When $\theta_B \lesssim \pi/17$, TBU is not reached within the simulation time of 60 s. Because evaporation is slower, the valley that develops in the AL is less pronounced, and the resulting peak in osmolarity is smaller; see Taranchuk and Braun [136] for more details.

3.1.1 Varying the Marangoni number

We now consider the effect of the Marangoni number on tear film dynamics as the director angle θ_B varies from 0 to $\pi/2$. Figure 3 shows the extreme values of AL thickness, osmolarity, and LL thickness for three values of the Marangoni number:

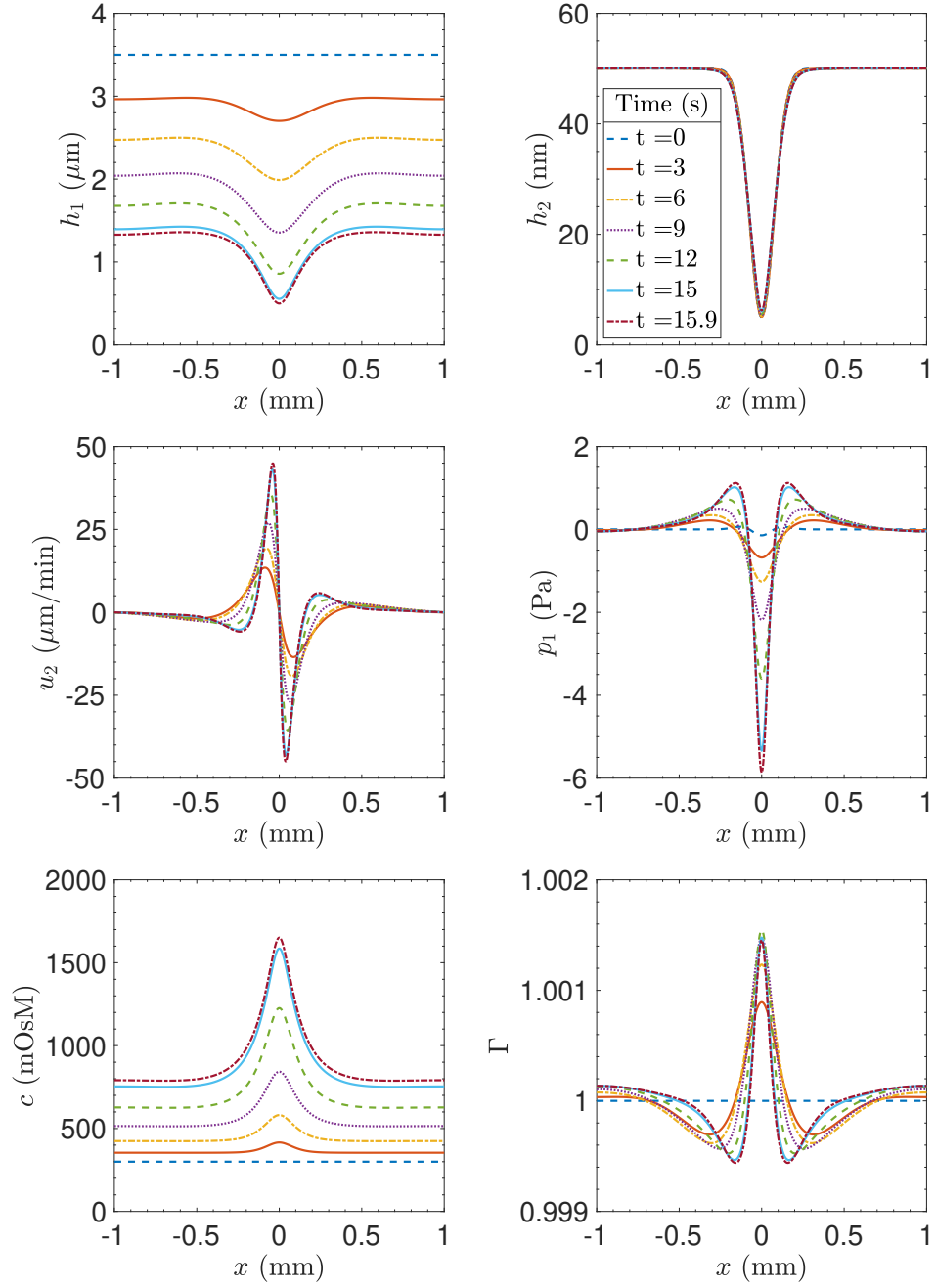


Fig. 2 Solutions for spatially-uniform initial conditions except for a Gaussian disturbance in the LL thickness. The director angle is $\theta_B = 0$. This figure illustrates typical dynamics of the dependent variables in space and time for the case of TBU driven by increased evaporation from the valley in the LL.

\mathcal{M} (the default value of 187.7), $\mathcal{M}/10$, and $10\mathcal{M}$. Solutions are also shown for the initial conditions of Section 2.2.2, the local excess of surfactant; these are described in further detail below in Section 3.2.1.

We see that when $\mathcal{M} \rightarrow \mathcal{M}/10$, the Marangoni effect is weakened, and there are no cases of TBU within 60 s. The LL is the most mobile in this case, as healing flow (driven by capillarity) allows the valley in the LL to thicken from its initial minimum of 5 nm, to local minima of 14.7 nm to 33.3 nm, depending on the angle of the director. Osmolarity decreases monotonically from 1323 mOsM to 467 mOsM.

For the default Marangoni number, TBU occurs before 60 s for $\theta_B \lesssim \pi/17$. Around this critical director angle the LL has some mobility, with the lipid valley thickening to a maximum of 17.2 nm; however, for $\theta_B \rightarrow \pi/2$, the LL moves very little from its initial profile.

When $\mathcal{M} \rightarrow 10\mathcal{M}$, TBU occurs before 60 s for $\theta_B \lesssim \pi/9$. The LL remains tangentially immobile for all angles of the director. Osmolarity decreases over the range of the θ_B , but its decline is slower than for the default Marangoni number.

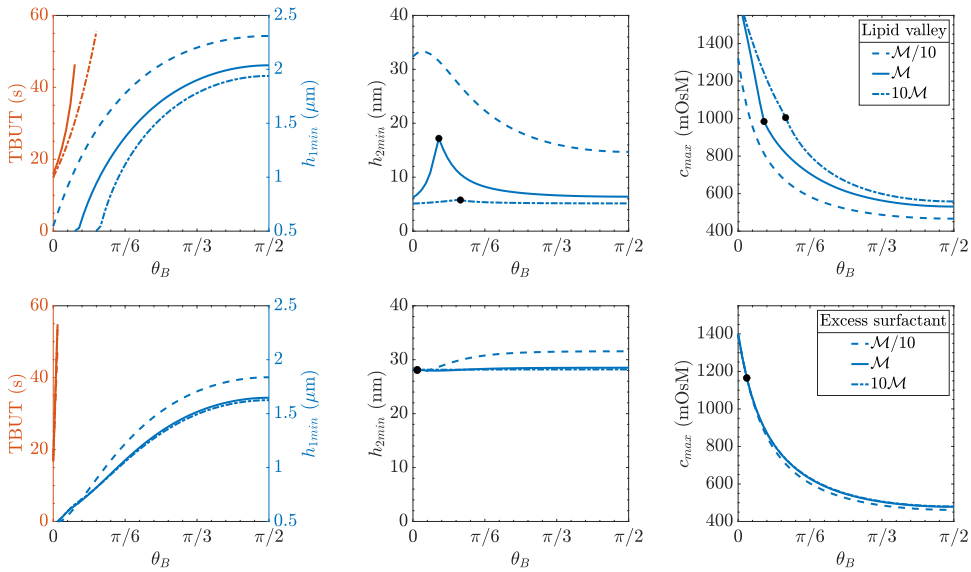


Fig. 3 Extreme values of AL thickness, osmolarity, and LL thickness at the final time as θ_B is varied from 0 to $\pi/2$, for three values of the Marangoni number \mathcal{M} . To the left of the black dots, TBUT occurs before 60 s; to the right, the simulations end at 60 s. The first row corresponds to the initial condition with a valley in the LL described in Section 2.2.1. The second row corresponds to the initial condition with a local excess of surfactant described in Section 2.2.2.

3.1.2 Varying the evaporative resistance parameter

Figure 4 shows the effect of varying \mathcal{R}_0 , the evaporative resistance parameter of the LL. The default value $\mathcal{R}_0 = 17.68$ is based on a nonlinear least squares fit to lipid thickness and permeability measurements performed by Stapf et al. [135]; this is shown

with the vertical dashed line. With this level of resistance, only a director angle of $\theta_B = 0$ results in a tear breakup time (TBUT) before 60 s. However, if \mathcal{R}_0 is decreased by a factor of 10, then TBU occurs in under 15 s for all values of the director angle. As the evaporative resistance parameter is increased, the minimum AL thickness tends toward the initial value of $3.5 \mu\text{m}$.

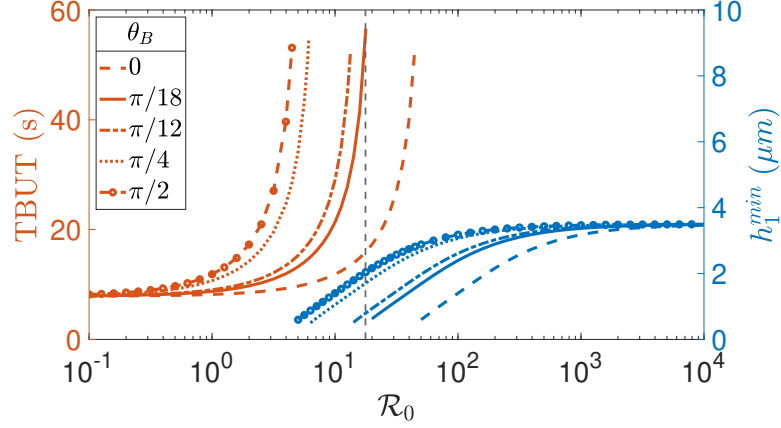


Fig. 4 Tear film breakup time or the minimum thickness of the AL after 60 s as a function of the evaporation resistance parameter \mathcal{R}_0 for the initial condition with a valley in the LL. The black dashed vertical line denotes the default value of $\mathcal{R}_0 = 17.68$.

3.1.3 The effect of liquid crystal viscosities on thinning

We have chosen to set the Leslie viscosities to three times the values of 5CB, a relatively well studied liquid crystal. By doing this, we match the dynamic viscosity of the LL, μ_2 , to previously used value of 0.1 Pa s [100, 135]. However, there is much uncertainty around the values for the Leslie viscosities as they have not been measured for the LL, and using a scale factor of 3 is only one possible choice. Thus, in Figure 5, we consider the effect of a wide range of scalings on the minimum values for both the aqueous and LL. Note that because we are scaling the dimensional quantities, in the nondimensional form we are effectively scaling μ_2 . Here we reduce the Marangoni number by a factor of 10 ($\mathcal{M} \rightarrow \mathcal{M}/10$) in order to isolate the effect of the liquid crystal viscosities on tear film thinning and breakup.

For values of μ_2 that are increased by less than a factor of 1000, there is little change in either the minimum AL thickness or LL thickness at the final time. For values of μ_2 more than a factor of 1000 larger than default, we begin to see breakup within 60 s for small values of θ_B . However, for larger director angles, the AL is fairly unaffected. On the other hand, for small values of μ_2 we observe a much more mobile LL for all orientations of the director. As μ_2 increases, the LL becomes immobile, and the minimum thickness remains close to the initial value of 5 nm.

Figure 6 shows solutions at the final time when μ_2 is increased by a factor of 2000. At this value, we see the most variation in LL thickness with respect to the director

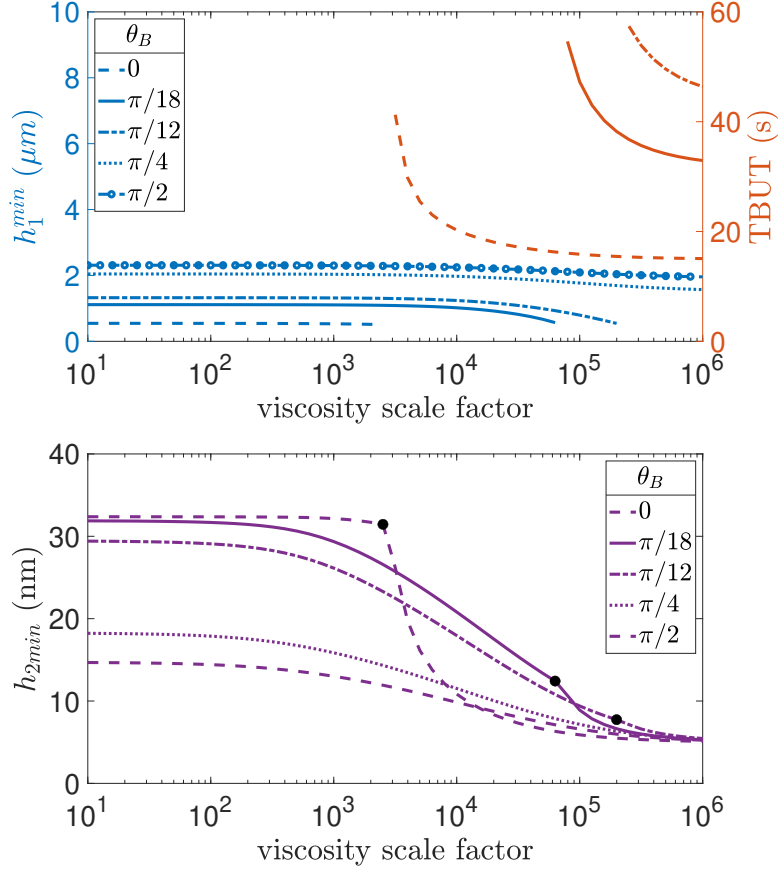


Fig. 5 Minimum thickness of the AL after 60 s or TBUT as a function of the scale factor applied to the 5CB liquid crystal parameters. To the left of the black dots, TBUT occurs before 60 s; to the right, the simulations end at 60 s.

angle. For clarity, we omit $\theta_B = \pi/18$ and $\pi/4$. When $\theta_B = \pi/2$, the minimum LL thickness is just over 12 nm, while when $\theta_B = 0$, the effects of capillarity result in healing flow, which increases the minimum thickness to 31.7 nm. For the intermediate value of $\theta_B = \pi/12$, the LL experiences some healing flow with a minimum of 24.1 nm, but mobility is reduced.

It is natural to explore an alternative scenario: keeping a scaling of three on α'_4 , which maintains $\mu_2 = 0.1$ Pa s, while scaling the other Leslie viscosities, α'_i , $i = 1, \dots, 6$, $i \neq 4$. By doing this, we are changing the coefficient A/B on the extensional term in Equation (4). Note that as $\alpha'_i \rightarrow 0$, $i = 1, \dots, 6$, $i \neq 4$, we return to the Newtonian limit, where $A/B = 4$. However, we find that if we increase the scaling too much (more than a factor of 16), the coefficient A/B becomes positive for some values of θ_B , making the problem ill-posed. In addition, the effect of the scalings in this feasible range is negligible for all variables. If we look at the coefficient A/B for

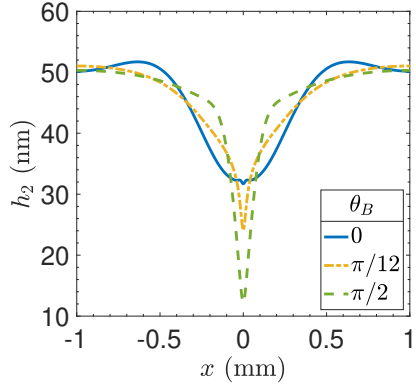


Fig. 6 Solutions for the LL at 60 s when the initial condition has a valley in the LL and $\mu_2 \rightarrow 2000 \mu_2$, and $\mathcal{M} \rightarrow \mathcal{M}/10$.

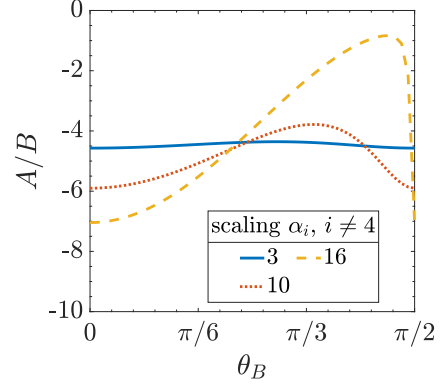


Fig. 7 The coefficient A/B as θ_B varies for scalings of 3, 10, and 16 on the Leslie viscosities α_i , $i = 1, \dots, 6$, $i \neq 4$ for the liquid crystal 5CB.

scalings, shown in Figure 7, we see that the change on the coefficient is very little, even with the maximum scale factor of 16.

3.2 Marangoni-driven thinning

We now turn to the initial conditions of Section 2.2.2, in which concentration gradients drive the tear film dynamics. The Marangoni effect results in rapid tangential flow; thus we consider solutions on a short timescale, shown in Figure 8, and a longer timescale, shown in Figure 9. Figure 8 shows the evolution of the variables over the first 0.06 s, when $\theta_B = \pi/2$. These solutions are representative of the dynamics of tear film thinning due to surfactant concentration gradients regardless of the orientation of the liquid crystal molecules; the director angle θ_B has little effect on the short timescale. The large surfactant gradients immediately cause rapid thinning in both the lipid and aqueous layers. As the local excess of surfactant flattens, the Marangoni effect concludes. The LL thins dramatically, with the valley thickness roughly half of the initial value of 50 nm. Fluid is pulled away from the excess surfactant, and builds up on the edges of the domain. The pattern of thinning is very similar in the AL, although to a lesser degree. During this initial redistribution of fluid, the LL fluid velocity is very large in magnitude (around $3 \times 10^5 \mu\text{m}/\text{min}$), but quickly slows to the range of $\pm 5 \mu\text{m}/\text{min}$ throughout the domain (not shown). Similarly, AL pressure (not shown) drops in magnitude from a range of $\pm 3 \text{ Pa}$ during the first 1 s, to $\pm 1 \text{ Pa}$, and thinning continues over a longer timescale.

Figure 9 shows solutions at the final time for five values of θ_B ranging from 0 to $\pi/2$. Breakup conditions are reached when $\theta_B = 0$ by 16.6 s; for all other values of θ_B , the final time of 60 s is reached. The surfactant concentration remains effectively uniform around 1.58 times the original background concentration, and over the longer timescale it is the evaporative resistance in the LL that influence thinning dynamics. When $\theta_B = \pi/2$ or $\pi/4$ thinning becomes more localized in the center of the domain, while smaller values of θ_B maintain a wider valley of thinning through time. For larger values of θ_B , we observe that negative pressure in the center of the AL domain pulls fluid in, and helps to reduce thinning. This results in an overall thicker AL at the final time. Arrows in the velocity and pressure plots of Figure 9 point to the difference in behavior when $\theta_B = \pi/4$ or $\pi/2$ as compared to smaller director angles.

On the other hand, the LL profiles are indistinguishable from each other at the final time and look very similar to the solution at 0.06 s shown in Figure 8. Virtually all of the movement in the LL happens within the first second; this immobilization of the fluid surface due to the Marangoni effect has been studied in other contexts such as vertical drainage in Braun et al. [149] and remobilization of droplet surfaces in Stebe and Maldarelli [150].

Osmolarity in the AL increases for all values of θ_B over the original value of 300 mOsM; however, it is most pronounced when $\theta_B = 0$. While the solutions in the AL are not dissimilar for $\theta_B = 0$ and $\theta_B = \pi/18$, the osmolarity is very different. When $\theta_B = 0$, peak osmolarity reaches nearly 1400 mOsM by 16.6 s, more than one and a half times the peak osmolarity at 60 s when $\theta_B = \pi/18$. When $\theta_B = 0$, thinning and TBU happen so rapidly that the solutes do not have enough time to diffuse through the AL.

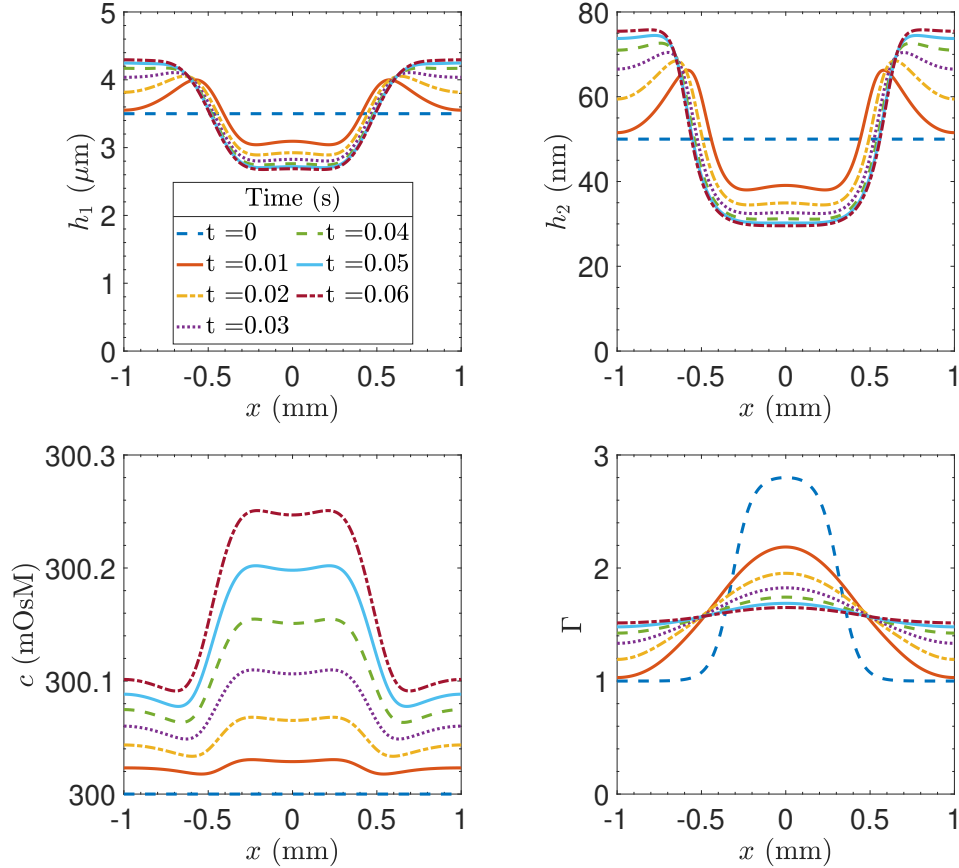


Fig. 8 Solutions on a short time scale for spatially-uniform initial conditions except for a local excess of surfactant. The director angle is $\theta_B = \pi/2$. This figure illustrates typical dynamics of the dependent variables in space and time. The surface gradients of surfactant drive all the dynamics.

3.2.1 Varying the Marangoni number

The second row of Figure 3 shows extreme values for AL thickness, osmolarity, and LL thickness as the director angle varies from 0 to $\pi/2$ for three values of the Marangoni number: the default \mathcal{M} (187.7), $\mathcal{M}/10$, and $10\mathcal{M}$. In general, compared to the initial condition with a valley in the LL which are discussed in Section 3.1.1, varying the Marangoni number has a much smaller effect on the variables. This is because with localized excess surfactant in the initial condition, the Marangoni effect is already driving dynamics, and our default Marangoni number is strong enough that increasing or decreasing by a factor of 10 does not have a dramatic effect.

For all three values of the Marangoni number, TBU occurs for $\theta_B < \pi/50$ when the initial condition has a local excess of surfactant. For larger director angles, there is no breakup within 60 s, but the AL thins much more than in the case with the lipid valley, with minimum AL thickness ranging from 1.62 to 1.84 μm when $\theta_B = \pi/2$.

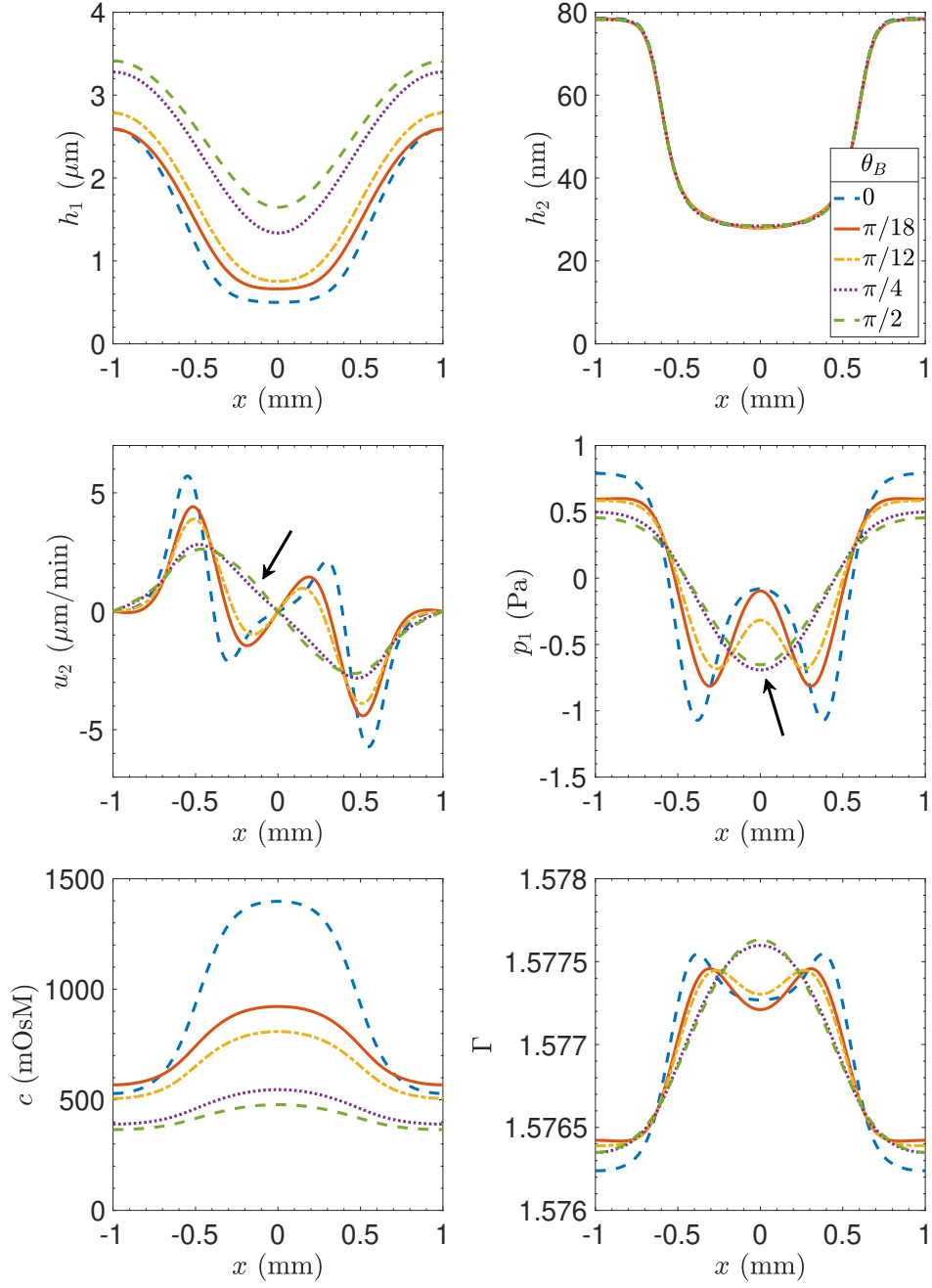


Fig. 9 Solutions at the final time for spatially-uniform initial conditions except for a local excess of surfactant. When $\theta_B = 0$, breakup occurs at 16.6 s; for all other values of θ_B the final time is 60 s. The LL profiles (upper right) are nearly identical for all θ_B .

After the initial rapid redistribution of fluid due to the Marangoni effect, the valley formed in the LL has a minimum value of 28 nm when $\theta_B = 0$ for all three cases. For \mathcal{M} and $10\mathcal{M}$ the minimum remains the same for all values of the director. For $\mathcal{M}/10$, the minimum increases slightly as the director angle increases, with a minimum value of 31.6 nm when $\theta_B = \pi/2$. Osmolarity between the three cases is very similar, with a maximum difference of 28 mOsM; in fact, the osmolarity curve for $10\mathcal{M}$ is indistinguishable from that of \mathcal{M} in Figure 3.

3.2.2 Varying the evaporative resistance parameter

We now explore the effect of the evaporative resistance parameter \mathcal{R}_0 . Figure 10 shows the TBU conditions as \mathcal{R}_0 varies for various orientations of the director. A small evaporative resistance parameter results in rapid thinning of the AL with breakup just under 5 s for all values of θ_B . As \mathcal{R}_0 increases, breakup time increases, until eventually the final time of 60 s is reached before breakup occurs. The value of \mathcal{R}_0 at which this occurs varies from 2.5 for $\theta_B = \pi/2$ to 25.1 for $\theta_B = 0$. The default value, denoted by the dashed vertical line, falls into this range where thinning may result in breakup before 60 s, depending on the director angle. See Figure 9 for solutions at the final time. As \mathcal{R}_0 becomes very large, evaporation is diminished, and the minimum value tends toward $3.1 \mu\text{m}$ for all values of θ_B .

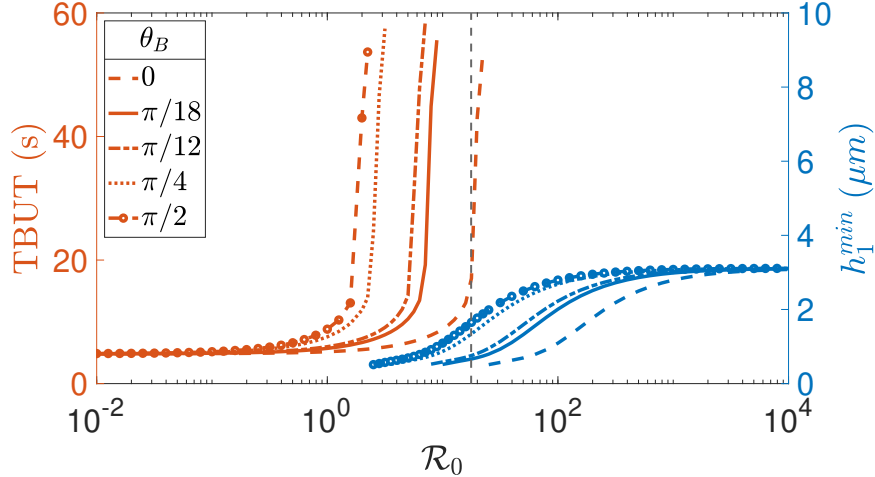


Fig. 10 Tear film breakup time or the minimum thickness of the AL after 60 s as a function of the evaporation resistance parameter \mathcal{R}_0 for the initial condition that has a local excess of surfactant. The black dashed vertical line denotes the default value of $\mathcal{R}_0 = 17.68$.

Figure 11 shows the relationship between the evaporative resistance parameter and the angle of the director for the two sets of initial conditions. The value of \mathcal{R}_0 which results in breakup conditions at 60 s is shown in red for $\theta_B = 0, \pi/18, \pi/12, \pi/4,$ and $\pi/2$. The circles represent the solution from the evaporation-driven flow caused by a valley in the LL; the crosses represents solutions from flow driven by the Marangoni

effect caused by localized excess surfactant. The black lines are rational functions fit to the respective data delineating whether or not breakup conditions are reached by the final time of 60 s. If the evaporative resistance parameter is decreased by a factor of 10 from the default value of 17.68, then TBU will occur for all angles of the director for both sets of initial conditions, although TBUT will vary.

If we compare the two curves, we see that the \mathcal{R}_0 which results in TBU at 60 s for the case of evaporation-driven thinning is roughly double that of the case of Marangoni-driven flow. In the evaporative case, when $\theta_B = 0$, the evaporative resistance parameter $\mathcal{R}_0 = 50$, whereas for the Marangoni-driven thinning, $\mathcal{R}_0 = 25$. When $\theta_B = \pi/2$, \mathcal{R}_0 is 5 and 2.5, respectively. This trend roughly holds for all values of the director angle. In general, this is expected behavior; the LL acts as a barrier to evaporation in part due to its thickness. In the first set of initial conditions, a deficiency in the LL leads to increased evaporation. Thus, it cannot tolerate an evaporation resistance parameter value of any less than 50 without TBU occurring before 60 s when $\theta_B = 0$. On the other hand, in the Marangoni-driven flow, the LL begins with a uniform thickness of 50 nm which helps to prevent TBU even though other aspects of the barrier may be compromised.

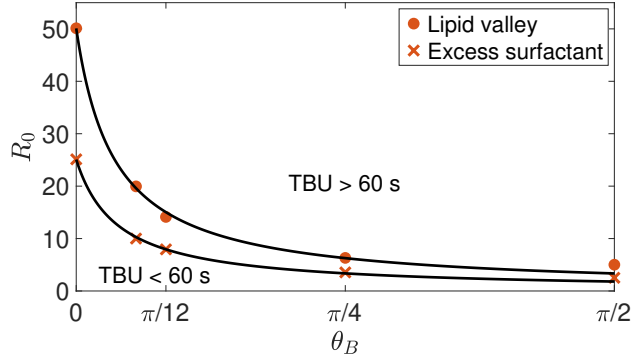


Fig. 11 A comparison of the \mathcal{R}_0 value which results in TBU at 60 s for two sets of initial conditions: one describing evaporation-driven flow (red circles), and one describing flow driven by the Marangoni effect (red crosses), as a function of the director angle of the liquid crystal molecules in the LL. The black lines are a fit to the respective data. To the left of each black line, TBU occurs before 60 s; to the right of each black line, TBU may occur after 60 s.

Table 4 Comparison of minimum AL thickness and maximum osmolarity when the initial LL thickness is reduced from 50 nm to 25 nm. The factor increase in peak osmolarity is compared to the ideal osmolarity of 300 mOsM.

θ_B	h_{1min}			c_{max}			
	50 nm (TBUT)	25 nm (TBUT)	% decrease	50 nm	factor \uparrow	25 nm	factor \uparrow
0	0.5 (16.6 s)	0.5 (8.2 s)	0	1398	4.66	1457	4.86
$\pi/18$	0.6626	0.5 (54.8 s)	24.5	922	3.07	1273	4.24
$\pi/12$	0.7538	0.5528	26.7	809	2.70	1134	3.78
$\pi/4$	1.3361	0.8010	40.1	546	1.82	768	2.56
$\pi/2$	1.6472	0.9926	39.7	478	1.59	659	2.20

3.2.3 Reducing initial lipid layer thickness

The thickness of the LL ranges between 20 - 120 nm, with more recent measurements favoring a thinner LL [140–142]. We halve the initial LL thickness from 50 nm (a “normal” tear film thickness), to 25 nm (a “thin” thickness). Figure 12 shows solutions for the AL and osmolarity at the final time for a few values of θ_B . The solutions can be compared with those of Figure 9 which show solutions for a 50 nm thick initial LL. Qualitatively, solutions for large values of θ_B are similar, although the AL is thinner, especially at its minimum. However, for $\theta_B = \pi/12$ or $\pi/18$, there are two minima, located symmetrically about the center. For $\theta_B = 0$, the region of thinning is steeper and more narrow than when the LL is thicker. In all cases, the solutions for osmolarity show higher concentrations with a thinner LL.

Table 4 shows that a 50% decrease in LL thickness results in a 40.1% decrease in the minimum AL thickness when $\theta_B = \pi/4$; for other values of the director, the percent decrease is even less. The factor increase in peak osmolarity over the ideal osmolarity is also shown. These numbers are highest when TBU occurs; however, with a thinner LL, peak osmolarity is well over twice the ideal value for all angles of the director.

Figure 13 shows the effect of varying the director angle by plotting parametric changes to the minimum value of the AL thickness and the maximum value of osmolarity at the final time as θ_B varies from 0 to $\pi/2$ for both a normal and thin LL. When the LL thickness is 50 nm, TBU occurs before 60 s only for values of $\theta_B < \pi/50$; when the LL thickness is 25 nm, TBU occurs for $\theta_B < \pi/14$. The black dots on the plot mark this change. Minimum LL thickness as θ_B varies is not shown, as changes are minimal. When the initial LL thickness is 50 nm, minimum values hovers near 28 nm; when the initial thickness is 25 nm, the minimum values remain around 14 nm for all values of the director angle.

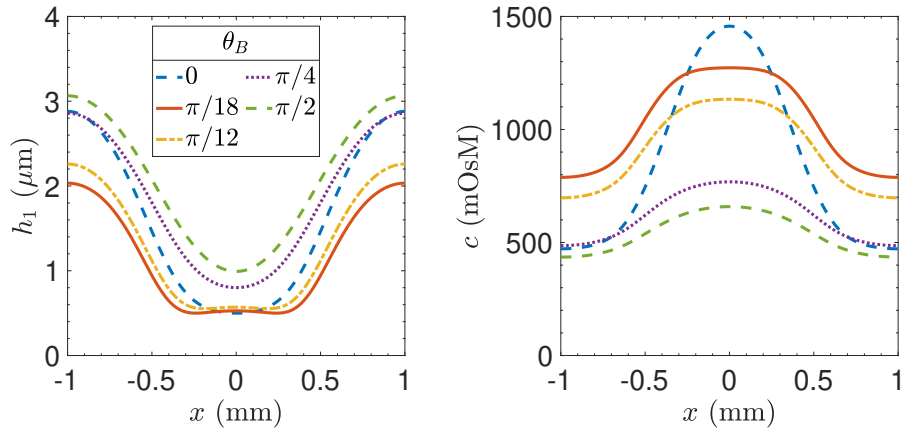


Fig. 12 Solutions at the final time for spatially-uniform initial conditions except for a local excess of surfactant. The initial thickness of the LL is 25 nm (half the default value). When $\theta_B = 0$, breakup occurs at 8.2 s; when $\theta_B = \pi/18$, breakup occurs at 54.8 s. For all other values of θ_B , the final time is 60 s.

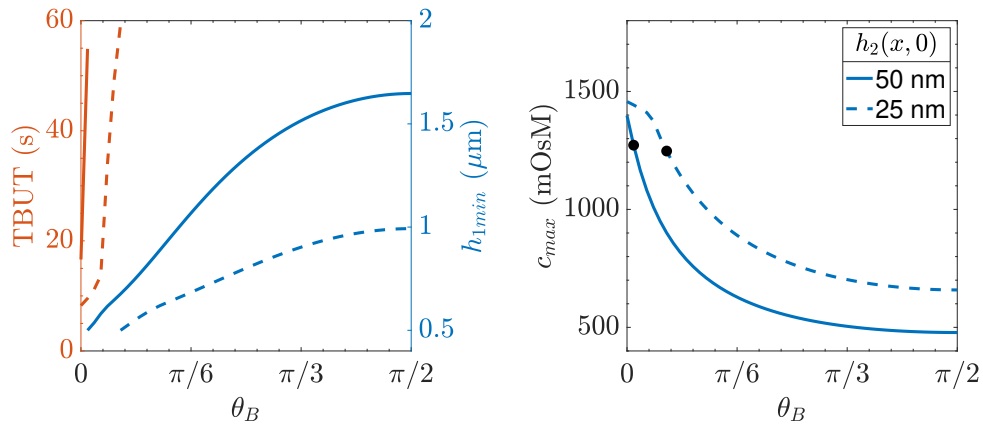


Fig. 13 Extreme values of AL thickness, osmolarity, and LL thickness at the end of each simulation as θ_B is varied from 0 to $\pi/2$. To the left of the black dot, TBUT occurs before 60 s; to the right of this dot, the simulations end at 60 s.

3.3 Combining lipid layer and surfactant perturbations

We now compare the two scenarios which combine perturbations in both the LL thickness and the surfactant concentration. The first combination is a bump in h_2 with a local excess of Γ , and the second is a valley in h_2 with a local excess of Γ . Figure 14 compares solutions for AL and LL thickness, as well as osmolarity for these two cases with $\theta_B = \pi/2$. While neither case reaches breakup for this angle of the director, thinning in the AL is more pronounced when there is a valley in the LL, with a minimum value of $0.94 \mu\text{m}$, as compared to $1.66 \mu\text{m}$ when the LL contains a bump. The LL behavior is similar in both cases; it undergoes rapid redistribution of fluid initially, and then remains tangentially immobile for the remainder of the time. When the LL contains a bump, this extra fluid is quickly redistributed throughout the domain; an area of thinning results, with the minimum thickness of 28.46 nm . When the LL contains a valley, the Marangoni effect magnifies this profile resulting in a solution similar to those of Figure 9, but with a deeper valley: the depth is now 14.15 nm versus 28.1 nm (when $\theta_B = \pi/2$).

Osmolarity in both cases reflects the respective changes in the AL. When the LL contains a valley, the AL thinning is more pronounced, and thus osmolarity reaches a peak of 650 mOsM , with little increase in concentration at the edges of the domain. When the LL contains a bump, the AL thins to a lesser degree, and the osmolarity steadily rises throughout the domain, with a smaller peak in the center. Peak osmolarity at the final time reaches 485 mOsM . In all scenarios that contain a local excess of surfactant initially, the Marangoni effect results in a rapid flattening of the surfactant concentration to a more or less uniform value of 1.58 .

We can consider the influence of the director angle, by observing the final time solutions for various angles as shown in Figure 15. When there is a bump in the LL, we see more variation resulting from changes in the director angle. When $\theta_B = 0$, TBU occurs at 46.8 s , but no other angles of the director result in breakup. When there is a valley in the LL, the director angle has less of an impact because rapid thinning in the AL leads to TBU for $\theta_B = 0, \pi/18, \text{ and } \pi/12$. Breakup times are detailed further in Table 5 which is discussed more below. Osmolarity at the final time is strongly influenced by the director angle. When there is a bump in the LL, peak osmolarity is almost three times higher for $\theta_B = 0$ (1409 mOsM) than for $\theta_B = \pi/2$ (485 mOsM). The difference is just over double when there is a valley in the LL (1442 versus 650 mOsM).

Thus far we have considered a valley in the LL with depth 25 nm in a 50 nm LL. We now vary this profile keeping a valley of half thickness. Table 5 compares the TBUT for three different LL background thicknesses: $30, 40, \text{ and } 50 \text{ nm}$. We see that the dynamics are not sensitive to LL thickness when $\theta_B = 0$. This is because evaporative resistance is at its lowest for this angle of the director; for all of the scenarios we have considered, $\theta_B = 0$ results in TBU before 60 s . LL thickness has a stronger effect for intermediate angles of the director. For example, when $\theta_B = \pi/18$, decreasing the LL thickness by 20% , from 50 nm to 40 nm , results in TBU in half the time. When θ_B is large enough, TBU does not occur; for all three LL thicknesses TBU does not occur for $\theta_B = \pi/4$ or $\pi/2$.

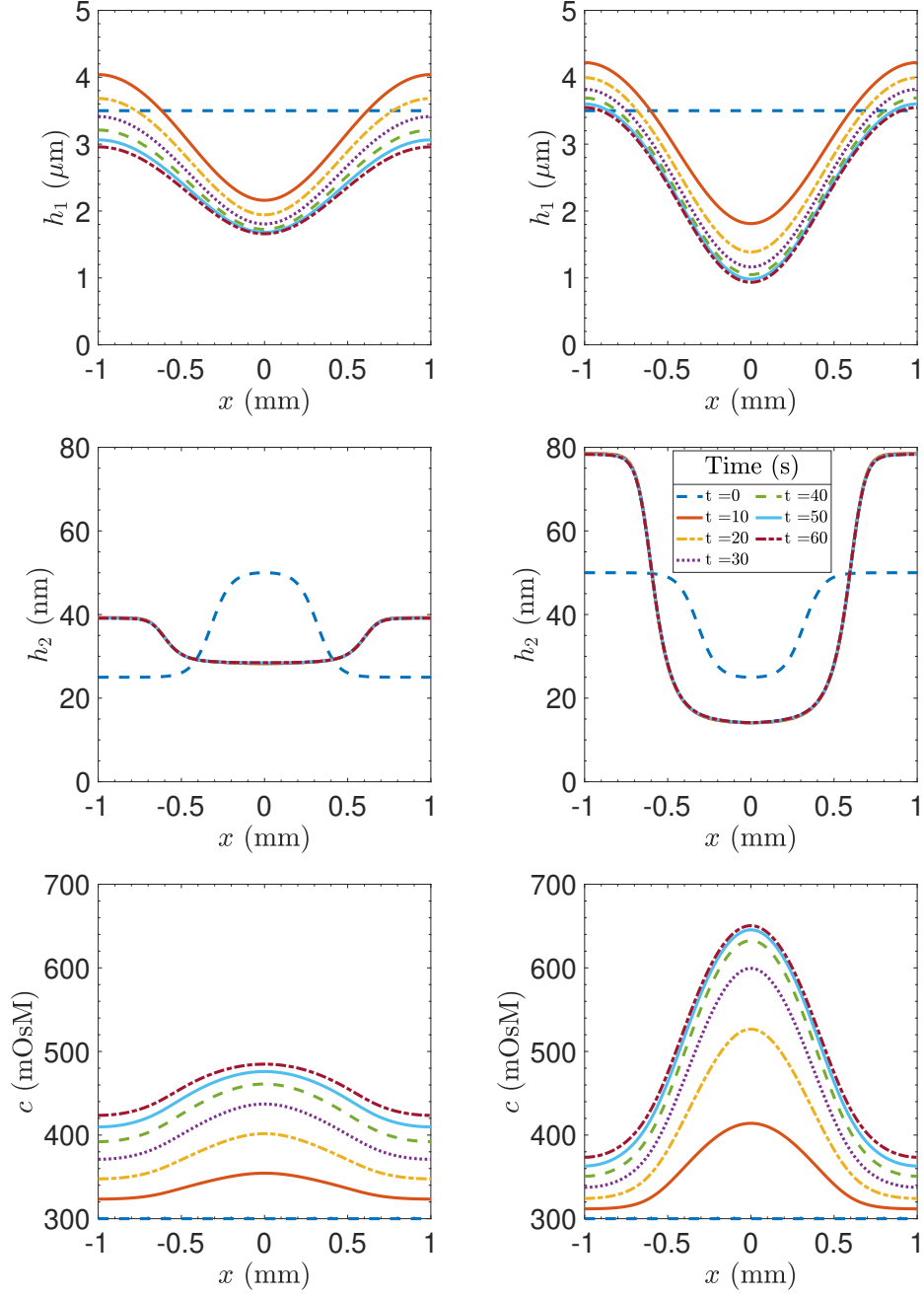


Fig. 14 Left column: Solutions when $\theta_B = \pi/2$ for a bump h_2 combined with a local excess of Γ . Right column: Solutions when $\theta_B = \pi/2$ for a valley in h_2 combined with a local excess of Γ . In both cases $\Gamma(x, 0)$ is given by Equation (16). The different $h_2(x, 0)$ appears in the middle row.

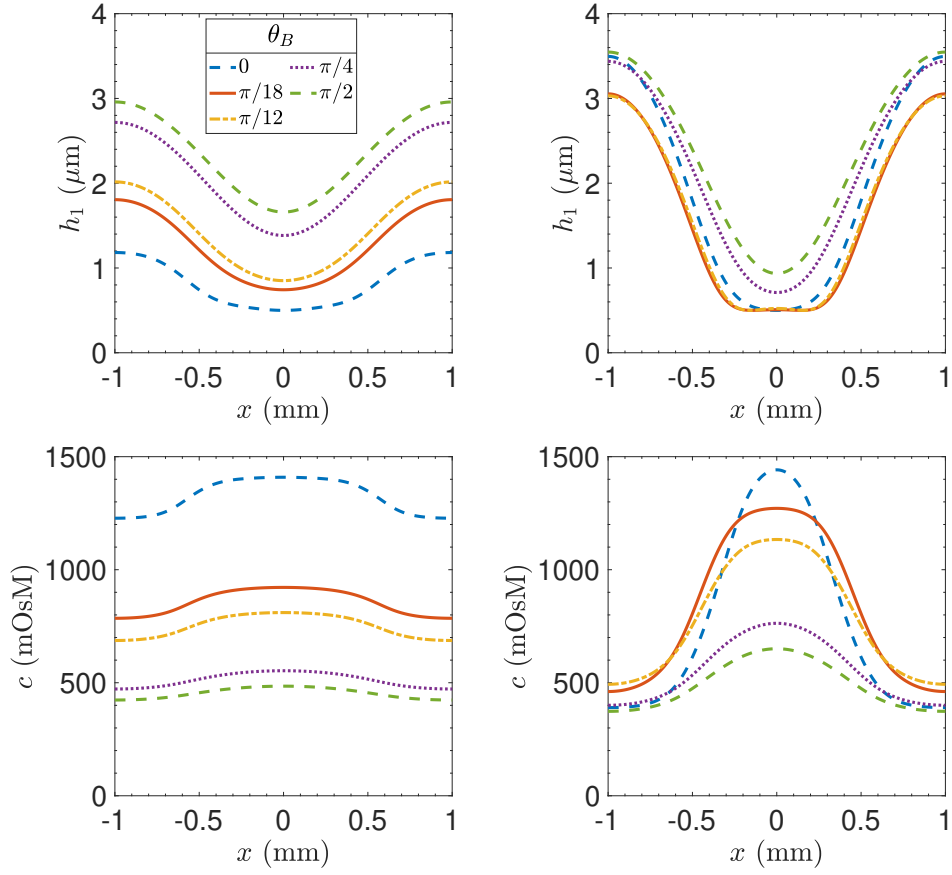


Fig. 15 Left column: Solutions at the final time for a bump in h_2 combined with a local excess of Γ . Right column: Solutions at the final time for a valley in h_2 combined with a local excess of Γ .

Table 5 TBU time comparison in seconds for various initial LL thicknesses when a valley in the LL is combined with a local excess of surfactant.

LL max/min (nm)	θ_B				
	0	$\pi/18$	$\pi/12$	$\pi/4$	$\pi/2$
50/25	8.2	29.6	48.4	-	-
40/20	7.4	15.0	32.2	-	-
30/15	6.7	10.7	14.3	-	-

4 Discussion and conclusion

In this paper we explore a new model for the tear film of the eye that was derived in Taranchuk and Braun [136]. This two-layer model combines a Newtonian AL with a nematic liquid crystal LL, and links molecular orientation of the LL with evaporative resistance that depends on the director angle. The LL acts as a barrier to evaporation of the AL, and thickness alone does not explain its role in preventing evaporation [127, 128]. By representing the LL as nematic liquid crystal, we are able to consider possible connections between the structure and composition of the LL and its affect on tear film thinning and breakup.

We examined two key drivers of TBU: evaporation and the Marangoni effect. We consider several scenarios which may lead to TBU. The first is a narrow valley in the LL, which leads to thinning of the AL due to increased evaporation. The second is a local excess of surfactant on the AL/LL interface, for which we see thinning on two timescales. Initially, surfactant gradients lead to rapid outward flow in both the AL and LL. The surfactant concentration levels out within the first second, and then evaporation takes over, continuing tear film thinning over a longer timescale of 60 s. Finally, we considered combinations of perturbations in both the LL and surface surfactant; one in which there is a bump in the LL combined with a local excess of surfactant, and one in which there is a valley in the LL combined with a local excess of surfactant. This final case depicts a worst case scenario, where both excess surfactant and a deficiency in the LL drive thinning, and breakup conditions are reached for $\theta_B \lesssim \pi/12$.

The evaporative resistance parameter \mathcal{R}_0 directly influences how quickly the AL thins. However, as shown in Figure 11, the minimum value of \mathcal{R}_0 that the system can tolerate while withstanding breakup also depends on the angle of the director, θ_B , and the initial condition for the LL. The evaporation function, given in Equations (9) and (10) and derived in A.3, shows one way these quantities may be related. While we have chosen to introduce director angle dependence in the evaporation function [29, 38, 151], we also see that the director angle has an effect on flow dynamics. Small angles of θ_B cause the LL to become more mobile, which results from liquid crystal properties in the LL.

In addition, we find that the default Marangoni number has a strong effect on dynamics, regardless of the initial conditions or other parameter values used. Thus, in order to observe the effect of the liquid crystal parameters, especially the Leslie viscosities, we reduce the Marangoni number by a factor of ten. In the absence of any measurements in the eye, we use the properties of 5CB as a starting point for the Leslie viscosities of the liquid crystal lipid layer. One unexpected finding is that varying the Leslie viscosities from the 5CB values has little effect on the dynamics. Not only that, but we are constrained in how much we can vary them, at least when using constant scalings of 5CB. On the other hand, the other main liquid crystal parameter θ_B , which describes the orientation of the molecules, affects both evaporation (by design), and flow. This is especially true for small angles.

Rather than varying all of the Leslie viscosities, we focused on varying α'_4 , which controls the dynamic viscosity of the LL (because $\mu_2 = \alpha'_4/2$). These results are very similar to the Newtonian case, explored in Stapf et al. [135], in that it takes a very

large increase in μ_2 to effect the dynamics of the AL. The director angle does have an effect on the mobility of the LL, until μ_2 become very large (on the order of 10^5). After this point, the LL becomes virtually tangentially immobile for all angles of the director.

Finally, we consider two initial conditions which combine perturbations in both the LL and the surface surfactant. The first is an undesirable case where a valley of lipid is combined with a local excess of surfactant. As expected, we see more breakup cases; for all angles of $\theta_B \lesssim 10$, TBU occurs within 60 s as a result of both the Marangoni effect and increased evaporation due to the deficiency in the LL.

Alternatively, we consider an initial condition which combines a bump in the LL with a local excess of surfactant. This scenario corresponds to Section 5.6 in Bruna and Breward [100], where in a limit h_2 and Γ can both be governed by the same equation. While we do not take that limit here, we model an initial condition in which the LL follows the surfactant. This area of increased thickness in the LL seem to be protective by creating a buffer against the Marangoni effect, and thus helping to prevent excessive thinning in the AL. Imaging of the LL has shown areas of varying thickness on occasion [22]. This type of initial condition could resemble this scenario, but more work is needed to link them.

Choudhury et al. [114] modeled TBU driven by dewetting due loss of mucins in the glycocalyx using a single layer model. They consider 119 s to be a normal time to breakup in a healthy eye, and their simulation resulted in TBU as short as 3.3 s when there is mucin loss over a third of the corneal surface. Dey et al. [112, 113] studied the same mechanism for TBU, but used a continuous-viscosity model which combined the mucus and aqueous layers. Their model predicted breakup in 2.4 to 135 s for scenarios representing pathological to healthy conditions, respectively. *in vivo* measurements for subjects with dry eye or other eye conditions have shown TBU times well under 10 s. In healthy subjects, TBU times may be longer, but would generally occur in less than two minutes [33, 37, 126].

While our model focuses on different mechanisms for thinning and breakup, TBU times from our simulations fall within a similar range as previous models and experiments. We consider that a healthy eye has high evaporative resistance, corresponding to a large director angle. For the scenarios we considered, a director angle of $\theta_B = \pi/4$, or $\pi/2$ did not result in breakup within 60 s. We did not compute time to TBU; however, at the end of 60 s, minimum AL thicknesses were well above the threshold value of $0.5 \mu\text{m}$ for these larger director angles. For small angles of the director in which evaporative resistance was low and there was a deficiency in the LL or an excess of surfactant, our model predicted breakup in as little as 6 to 10 s. These predicted breakup times are not as rapid as the shortest TBU times observed in eyes [33, 126].

Thinning and breakup due to a glob surfactant was studied in Zhong et al. [30, 111]. The glob consisted of an interval of fixed concentration as well a part that was transported outside this interval. This area of fixed concentration, which acted as a source, was varied in size, and found to cause TBU either under or at the edge of the glob depending on size. TBU occurred in < 1 s to 15 s, and it was noted that evaporation aided TBU. Our results have central breakup and evaporation aligns with the Marangoni effect to promote TBU. Although our TBU time is on the longer

end of the range they predicted, our treatment of surfactant is simpler. We conserve surfactant, and the local excess of surfactant does not act as a source; nor did we experiment with larger or smaller concentrations.

Thinning due to evaporation has been modeled previously both with a fixed evaporation distribution [61], and with a static LL [46]. Alternatively, Luke et al. [54] developed an evaporation-driven model that was fit to experimental data. We have taken a mechanistic approach, and incorporated LL thickness, permeability, and structure in our evaporation function.

We have studied a variety of initial conditions and explored the effects of several key parameters on tear film dynamics when modeling the LL as nematic liquid crystal. Now that we have a sense of the key features and limitations of this model, future work could include a moving end to imitate the eyelid during a blink. Tear breakup is often related to the LL pattern [10, 126]; more fidelity would require a moving domain [97]. In addition, it would be valuable to determine more rheological properties for this kind of model [70–72].

Acknowledgements

This material is based upon work supported by the University of Delaware Graduate College through the Doctoral Fellowship for Excellence (MJT). Any opinions, findings, and conclusions or recommendations expressed in this material are those of the authors. RJB is grateful for SHD’s mentoring and many examples of the right way to do things. Remembering how he got his unofficial middle name, we have joined words wherever a possibility of using a hyphen has occurred in this paper.

Declarations

Competing interests

The authors have no competing interests to declare that are relevant to the content of this article.

Appendix A Dimensional equations

We give the dimensional equations (after [136]) and a very brief outline of the derivation.

A.1 Governing equations

Inside the AL, $0 < y' < h'_1$, we have conservation of mass and momentum using the Navier-Stokes equations. The advection-diffusion equation governs osmolarity transport within the AL. The equations in dimensional form with a prime denoting a dimensional quantity, respectively, are:

$$\nabla' \cdot \mathbf{u}'_1 = 0, \tag{A1}$$

$$\rho_1(\mathbf{u}'_{1t} + \mathbf{u}'_1 \cdot \nabla' \mathbf{u}'_1) = -\nabla' p'_1 + \mu_1 \Delta' \mathbf{u}'_1, \tag{A2}$$

$$c'_{t'} + \mathbf{u}'_1 \cdot \nabla' c' - D_1 \Delta' c' = 0, \quad (\text{A3})$$

where the divergence of \mathbf{u}'_1 is $\nabla' \cdot \mathbf{u}'_1 = u'_{1x'} + v'_{1y'}$, the gradient is $\nabla' \mathbf{u}'_1 = \begin{bmatrix} u'_{1x'} & v'_{1x'} \\ u'_{1y'} & v'_{1y'} \end{bmatrix}$, and the Laplacian of the first component of \mathbf{u}'_1 is $\Delta' u'_1 = u'_{1x'x'} + u'_{1y'y'}$.

Inside the LL, $h'_1 < y' < h'$, we have conservation of energy, mass, and momentum using the Ericksen-Leslie equations for liquid crystals.

$$\frac{\partial}{\partial x'} \left(\frac{\partial W'}{\partial \theta_{x'}} \right) + \frac{\partial}{\partial y'} \left(\frac{\partial W'}{\partial \theta_{y'}} \right) - \frac{\partial W'}{\partial \theta} + \tilde{g}'_x \frac{\partial n_x}{\partial \theta} + \tilde{g}'_y \frac{\partial n_y}{\partial \theta} = 0, \quad (\text{A4})$$

$$-\frac{\partial \pi'}{\partial x'} + \tilde{g}'_x \frac{\partial n_x}{\partial x'} + \tilde{g}'_y \frac{\partial n_y}{\partial x'} + \frac{\partial \tilde{t}'_{xy}}{\partial y'} + \frac{\partial \tilde{t}'_{xx}}{\partial x'} = 0, \quad (\text{A5})$$

$$-\frac{\partial \pi'}{\partial y'} + \tilde{g}'_x \frac{\partial n_x}{\partial y'} + \tilde{g}'_y \frac{\partial n_y}{\partial y'} + \frac{\partial \tilde{t}'_{yx}}{\partial x'} + \frac{\partial \tilde{t}'_{yy}}{\partial y'} = 0, \quad (\text{A6})$$

$$\frac{\partial u'_2}{\partial x'} + \frac{\partial v'_2}{\partial y'} = 0, \quad (\text{A7})$$

where, working in two dimensions,

$$\tilde{g}'_i = -\gamma_r N'_i - \gamma_t e'_{ik} n_k, \quad e'_{ij} = \frac{1}{2} \left(\frac{\partial u'_i}{\partial x'_j} + \frac{\partial u'_j}{\partial x'_i} \right), \quad (\text{A8})$$

$$N'_i = \dot{n}'_i - \omega'_{ik} n_k, \quad \omega'_{ij} = \frac{1}{2} \left(\frac{\partial u'_i}{\partial x'_j} - \frac{\partial u'_j}{\partial x'_i} \right), \quad \pi' = p'_2 + W', \quad (\text{A9})$$

$$W' = \frac{1}{2} \left[K_1 (\nabla' \cdot \mathbf{n})^2 + K_3 ((\mathbf{n} \cdot \nabla') \mathbf{n}) \cdot ((\mathbf{n} \cdot \nabla') \mathbf{n}) \right], \quad (\text{A10})$$

$$\tilde{t}'_{ij} = \alpha'_1 n_k n_p e'_{kp} n_i n_j + \alpha'_2 N'_i n_j + \alpha'_3 N'_j n_i + \alpha'_4 e'_{ij} + \alpha'_5 e'_{ik} n_k n_j + \alpha'_6 e'_{jk} n_k n_i. \quad (\text{A11})$$

We use summation notation here as it is standard when working with the Ericksen-Leslie equations, with $i, j, k = 1, 2$, and \dot{n}'_i denotes the convective derivative of the i th component of \mathbf{n} . We further assume that the elastic constants are equal; that is $K = K_1 = K_3$. These liquid crystal quantities are defined further in Table A1.

A.2 Boundary conditions

We now list the boundary conditions, proceeding from the cornea out towards the air. At $y' = 0$, we have velocity continuity and a no flux boundary condition for osmolarity transport. These are, respectively:

$$\mathbf{u}'_1 = \mathbf{J}_0, \quad (\text{A12})$$

$$c'(\mathbf{u}'_1 - \mathbf{s}'_{0t'}) - D_1 \nabla' c' = 0. \quad (\text{A13})$$

Note that as we assume the cornea is flat, $\mathbf{s}'_{0t'} = \mathbf{0}$.

Table A1 Liquid crystal variables and parameters [144].

Quantity	Description
$\mathbf{n} = (\sin \theta, \cos \theta)$	director field
$\theta(x', y', t')$	angle the director angle makes with the y -axis
p'_2	pressure in LL
W'	bulk energy density
$\pi' = p'_2 + W'$	modified pressure
\tilde{g}'_i	viscous dissipation
e'_{ij}	rate of strain tensor
N'_i	co-rotational time flux of the director \mathbf{n}
ω'_{ij}	vorticity tensor
τ'_{2ij}	viscous stress tensor
τ'_{2ij}	elastic stress tensor
τ'_2	stress tensor
$\alpha'_i, i = 1, \dots, 6$	Leslie viscosities (Newtonian: $\mu' = \alpha'_4/2$, all other $\alpha'_i = 0$)
$\gamma'_r = \alpha'_3 - \alpha'_2$	rotational/twist viscosity
$\gamma'_t = \alpha'_6 - \alpha'_5$	torsion coefficient
K_1, K_3	elastic constants for splay and bend respectively

At $y' = h'_1$, we have velocity continuity, aqueous and lipid mass conservation, and the stress balance. In addition, we have a no flux boundary condition for osmolarity transport, and the anchoring boundary condition for the LL. The equations, respectively, are:

$$(\mathbf{u}'_1 - \mathbf{u}'_2) \cdot \hat{t}'_1 = 0, \quad (\text{A14})$$

$$\rho_1(\mathbf{u}'_1 - \mathbf{s}'_{1t'}) \cdot \hat{n}'_1 = J'_e, \quad (\text{A15})$$

$$\rho_2(\mathbf{s}'_{1t'} - \mathbf{u}'_2) \cdot \hat{n}'_1 = 0, \quad (\text{A16})$$

$$(\tau'_{11} - \tau'_{22}) \cdot \hat{n}'_1 = -\gamma'_{s1} \hat{n}'_1 \nabla' \cdot \hat{n}'_1 + \nabla'_{s1} \gamma'_{s1}, \quad (\text{A17})$$

$$c'(\mathbf{u}'_1 - \mathbf{s}'_{1t'}) - D_1 \nabla' c' = 0, \quad (\text{A18})$$

$$\theta = \theta_B. \quad (\text{A19})$$

To resolve the stress balance into tangential and normal stress components, we take the dot product of the stress balance and \hat{t}'_1 or \hat{n}'_1 respectively. Here $\nabla'_{s1} = (\mathbf{I} - \hat{n}'_1 \hat{n}'_1) \cdot \nabla'$ is the surface gradient, where \mathbf{I} is the identity matrix [152].

At $y' = h'$, we have lipid mass conservation, stress balance, and anchoring respectively:

$$\rho_2(\mathbf{u}'_2 - \mathbf{s}'_{2t'}) \cdot \hat{n}'_2 = 0, \quad (\text{A20})$$

$$\tau'_{22} \cdot \hat{n}'_1 = -\gamma'_2 \hat{n}'_2 \nabla' \cdot \hat{n}'_2, \quad (\text{A21})$$

$$\theta = \theta_B. \quad (\text{A22})$$

The stress balance can be resolved into components in the same way as above, using the unit tangent and normal vectors at this interface, \hat{t}'_2 and \hat{n}'_2 .

At the aqueous-lipid interface $y' = h'_1$, we have surfactant transport and the linear equation of state for the surface tension, respectively:

$$\Gamma'_{t'} + \nabla'_{s_1} \cdot (\Gamma' u'_1) = D_s \nabla'^2_{s_1} \Gamma', \quad (\text{A23})$$

$$\gamma'_{s_1} = \gamma_1 - RT_0 \Gamma'. \quad (\text{A24})$$

A.3 Osmosis and evaporation

The effect of osmosis is determined by the difference in concentration on either side of the aqueous-corneal interface $y' = 0$,

$$\mathbf{J}'_0 \cdot \hat{n}'_0 = P_c (c' - c_0). \quad (\text{A25})$$

Here we assume an ideal osmolarity ($c_0 = 300$ mOsM) on the corneal side of the interface.

To account for the effect of evaporation at the aqueous-lipid interface $y' = h'_1$, we modify a boundary layer model derived thoroughly in Stapf et al. [135]

$$J'_e = \frac{E_0}{1 + \frac{k_m}{Dk} h'_2}. \quad (\text{A26})$$

Here, Dk represents resistance to evaporation provided by the LL based on its thickness and permeability. Its value comes from a nonlinear least squares fit to clinical data [34] performed by Stapf et al. [135], which is very similar to that of Cerretani et al. [123]. We further modify Dk to include a dependence on the director angle of liquid crystals in the LL. We suggest the orientation of the molecules affects evaporation through

$$J'_e = \frac{E_0}{1 + \frac{k_m}{Dk} (0.1 + 0.9 \sin \theta_B) h'_2}. \quad (\text{A27})$$

The maximum evaporation rate occurs when $\theta_B = 0$, which is ten times that of the rate for $\theta_B = \pi/2$. The minimum rate matches that used in [135].

A.4 Deriving the leading order system

We nondimensionalize using the scalings in (1), along with

$$W' = \frac{K}{\delta^2 L^2} W, \quad \alpha'_i = \mu_2 \alpha_i, \quad \gamma'_t = \mu_2 \gamma_t, \quad \gamma'_r = \mu_2 \gamma_r.$$

Then, we asymptotically expand all the dependent variables in powers of the small parameter $\epsilon \ll 1$. For example,

$$\Gamma(x, t) \sim \Gamma_0(x, t) + \epsilon \Gamma_1(x, t) + \epsilon^2 \Gamma_2(x, t) + \dots$$

We substitute these expansions into the nondimensionalized equations and collect like powers of ϵ . At leading order, we are able to determine the director angle, conservation of mass in both the AL and LL, and conservation of surfactant concentration. At $O(\epsilon)$, we are only able to determine intermediate variables, so we proceed to $O(\epsilon^2)$. We are then able to determine the AL depth averaged velocity, AL pressure, the force balance equation for the axial velocity in the LL, and conservation of osmolarity. This gives us the closed system of equations from Section 2.1. This progression is typical of problems like this [100, 135].

References

- [1] Bron, A.J., Tiffany, J.M., Gouveia, S.M., Yokoi, N., Voon, L.W.: Functional aspects of the tear film lipid layer. *Exp. Eye Res.* **78**, 347–360 (2004)
- [2] Smith, J.A., *et al.*: The epidemiology of dry eye disease: Report of the Epidemiology Subcommittee of the International Dry Eye WorkShop. *Ocul. Surf.* **5**, 93–107 (2007)
- [3] Stapleton, F., Alves, M., Bunya, V.Y., Jalbert, I., Lekhanont, K., Malet, F., Na, K.-S., Schaumberg, D., Uchino, M., Vehof, J., Viso, E., Vitale, S., Jones, L.: TFOS DEWS-II epidemiology report. *Ocul. Surf.* **15**(3), 334–365 (2017)
- [4] Lemp, M.A.: Report of the National Eye Institute/Industry workshop on Clinical Trials in Dry Eyes. *CLAO J* **21**, 221–232 (1995)
- [5] Lemp, M.A., *et al.*: The definition and classification of dry eye disease: Report of the Definition and Classification Subcommittee of the International Dry Eye WorkShop. *Ocul. Surf.* **5**, 75–92 (2007)
- [6] Craig, J.P., Nichols, K.K., Akpek, E.K., Caffery, B., Dua, H.S., Joo, C.-K., Liu, Z., Nelson, J.D., Nichols, J.J., Tsubota, K., *et al.*: TFOS DEWS-II definition and classification report. *Ocul. Surf.* **15**(3), 276–283 (2017)
- [7] Willcox, M.D.P., Arguëso, P., Georgiev, G.A., Holopainen, J.M., Laurie, G.W., Millar, T.J., Papas, E.B., Rolland, J.P., Schmidt, T.A., Stahl, U., Suarez, T., Subbaraman, L.N., Ucakhan, O.O., Jones, L.W.: TFOS DEWS-II Tear Film Report. *Ocul. Surf.* **15**(3), 369–406 (2017)
- [8] Baudouin, C., Aragona, P., Messmer, E.M., Tomlinson, A., Calonge, M., Boboridis, K.G., Akova, Y.A., Geerling, G., Labetoulle, M., Rolando, M.: Role of hyperosmolarity in the pathogenesis and management of dry eye disease: Proceedings of the OCEAN group meeting. *Ocul. Surf.* **11**, 246–258 (2013)
- [9] Tsubota, K.: Tear dynamics and dry eye. *Prog. Retin. Eye Res.* **17**(4), 565–596 (1998)
- [10] Braun, R.J., King-Smith, P.E., Begley, C.G., Li, L., Gewecke, N.R.: Dynamics

- and function of the tear film in relation to the blink cycle. *Prog. Retin. Eye Res.* **45**, 132–164 (2015)
- [11] Mishima, S., Maurice, D.M.: The oily layer of the tear film and evaporation from the corneal surface. *Exp. Eye Res.* **1**, 39–45 (1961)
- [12] Svitova, T.F., Lin, M.C.: Evaporation retardation by model tear-lipid films: The roles of film aging, compositions and interfacial rheological properties. *Coll. Surf. B: Biointerfaces* **197**, 111392 (2021)
- [13] Norn, M.S.: Semiquantitative interference study of the fatty layer of precorneal film. *Acta Ophthalmol.* **57**, 766–774 (1979)
- [14] Berger, R.E., Corrsin, S.: A surface tension gradient mechanism for driving the pre-corneal tear film after a blink. *J. Biomech.* **7**, 225–38 (1974)
- [15] Craster, R.V., Matar, O.K.: Dynamics and stability of thin liquid films. *Rev. Mod. Phys.* **81**(3), 1131 (2009)
- [16] Holly, F.J.: Formation and rupture of the tear film. *Exp. Eye Res.* **15**, 515–525 (1973)
- [17] Tiffany, J.M.: Measurement of wettability of the corneal epithelium: I. particle attachment method. *Acta Ophthalmol.* **68**(2), 175–181 (1990)
- [18] Tiffany, J.M.: Measurement of wettability of the corneal epithelium: II. contact angle method. *Acta Ophthalmol.* **68**(2), 182–187 (1990)
- [19] Gipson, I.K.: Distribution of mucins at the ocular surface. *Exp. Eye Res.* **78**, 379–388 (2004)
- [20] King-Smith, P.E., Fink, B.A., Hill, R.M., Koelling, K.W., Tiffany, J.M.: The thickness of the tear film. *Curr. Eye Res.* **29**, 357–368 (2004)
- [21] Yokoi, N., Takehisa, Y., Kinoshita, S.: Correlation of tear lipid layer interference patterns with the diagnosis and severity of dry eye. *Am. J. Ophthalmol.* **122**, 818–824 (1996)
- [22] Goto, E., Tseng, S.C.G.: Kinetic analysis of tear interference images in aqueous tear deficiency dry eye before and after punctal occlusion. *Invest. Ophthalmol. Vis. Sci.* **44**, 1897–1905 (2003)
- [23] King-Smith, P.E., Nichols, J.J., Nichols, K.K., Braun, R.J.: A high resolution microscope for imaging the lipid layer of the tear film. *Ocul. Surf.* **9**(4), 197–211 (2011)
- [24] Govindarajan, B., Gipson, I.K.: Membrane-tethered mucins have multiple functions on the ocular surface. *Exp. Eye Res.* **90**, 655–693 (2010)

- [25] Owens, H., Phillips, J.: Spreading of the tears after a blink: Velocity and stabilization time in healthy eyes. *Cornea* **20**, 484–487 (2001)
- [26] King-Smith, P.E., Nichols, J.J., Nichols, K.K., Fink, B.A., Braun, R.J.: Contributions of evaporation and other mechanisms to tear film thinning and breakup. *Optom. Vis. Sci.* **85**, 623–630 (2008)
- [27] Norn, M.S.: Dessication of the precorneal film. I Corneal wetting-time. *Acta Ophthalmol.* **47**, 865–80 (1969)
- [28] Lemp, M.A., *et al.*: The definition and classification of dry eye disease: Report of the Definition and Classification Subcommittee of the International Dry Eye WorkShop. *Ocul. Surf.* **5**, 75–92 (2007)
- [29] King-Smith, P.E., Begley, C.G., Braun, R.J.: Mechanisms, imaging and structure of tear film breakup. *Ocul. Surf.* **16**, 4–30 (2018)
- [30] Zhong, L., Braun, R.J., Begley, C.G., King-Smith, P.E.: Dynamics of fluorescent imaging for rapid tear thinning. *Bull. Math. Biol.* **81**, 39–80 (2019)
- [31] Zhang, Y.L., Matar, O.K., , Craster, R.V.: Analysis of tear film rupture: Effect of non-newtonian rheology. *J. Colloid Interface Sci.* **262**, 130–148 (2003)
- [32] Zhang, Y.L., Matar, O.K., , Craster, R.V.: Rupture analysis of the corneal mucus layer of the tear film. *Mol. Simul.* **30**, 167–172 (2004)
- [33] Yokoi, N., Georgiev, G.A.: Tear-film-oriented diagnosis for dry eye. *Japan. J. Ophthalmol.* **63**, 127–136 (2019)
- [34] King-Smith, P.E., Hinel, E.A., Nichols, J.J.: Application of a novel interferometric method to investigate the relation between lipid layer thickness and tear film thinning. *Invest. Ophthalmol. Vis. Sci.* **51**, 2418–23 (2010)
- [35] Sharma, A., Ruckenstein, E.: Mechanism of tear film rupture and formation of dry spots on cornea. *J. Coll. Interface Sci.* **106**, 12–27 (1985)
- [36] Sharma, A., Khanna, R., Reiter, G.: A thin film analog of the corneal mucus layer of the tear film: an enigmatic long range non-classical DLVO interaction in the breakup of thin polymer films. *Coll. Surf. B* **14**, 223–35 (1999)
- [37] Begley, C.G., Simpson, T., Liu, H., Salvo, E., Wu, Z., Bradley, A., Situ, P.: Quantitative Analysis of Tear Film Fluorescence and Discomfort During Tear Film Instability and Thinning. *Invest. Ophthalmol. Vis. Sci.* **54**(4), 2645–2653 (2013)
- [38] King-Smith, P.E., Bailey, M.D., Braun, R.J.: Four characteristics and a model of an effective tear film lipid layer. *Ocul. Surf.* **11**, 1–10 (2013)

- [39] Luke, R.A., Braun, R.J., Driscoll, T.A., Awisi-Gyau, D., Begley, C.G.: Parameter Estimation for Mixed-Mechanism Tear Film Thinning. *Bull. Math. Biol.* **83**(5), 56 (2021)
- [40] Doane, M.G.: Blinking and the mechanics of the lacrimal drainage system. *Ophthalmol.* **88**, 844–851 (1981)
- [41] Tomlinson, A., Doane, M.G., McFayden, A.: Inputs and outputs of the lacrimal system: Review of production and evaporative loss. *Ocul. Surf.* **7**, 17–29 (2009)
- [42] Kimball, S.H., King-Smith, P.E., Nichols, J.J.: Evidence for the major contribution of evaporation to tear film thinning between blinks. *Invest. Ophthalmol. Vis. Sci.* **51**, 6294–97 (2010)
- [43] Braun, R.J.: Dynamics of the tear film. *Annu. Rev. Fluid Mech.* **44**, 267–297 (2012)
- [44] Cerretani, C.F., Radke, C.J.: Tear dynamics in healthy and dry eyes. *Curr. Eye Res.* **39**, 580–595 (2014)
- [45] Stahl, U., Willcox, M., Stapleton, F.: Osmolality and tear film dynamics. *Clin. Exp. Optom.* **95**, 3–11 (2012)
- [46] Peng, C.-C., Cerretani, C., Braun, R.J., Radke, C.J.: Evaporation-driven instability of the precorneal tear film. *Adv. Colloid Interface Sci.* **206**, 250–264 (2014)
- [47] Lemp, M.A., Bron, A.J., Baudouin, C., Castillo, J.M.B., Geffen, D., Tauber, J., Foulks, G.N., Pepose, J.S., Sullivan, B.D.: Tear osmolarity in the diagnosis and management of dry eye disease. *Am. J. Ophthalmol.* **151**(5), 792–798 (2011)
- [48] Tomlinson, A., Khanal, S., Ramaesh, K., Diaper, C., McFadyen, A.: Tear film osmolarity: determination of a referent for dry eye diagnosis. *Invest. Ophthalmol. Vis. Sci.* **47**(10), 4309–4315 (2006)
- [49] Versura, P., Profazio, V., Campos, E.: Performance of tear osmolarity compared to previous diagnostic tests for dry eye diseases. *Curr. Eye Res.* **35**(7), 553–564 (2010)
- [50] Gilbard, J.P., Farris, R.L., Santamaria, J.: Osmolarity of tear microvolumes in keratoconjunctivitis sicca. *Arch. Ophthalmol.* **96**, 677–681 (1978)
- [51] Sullivan, B.D., Whitmer, D., Nichols, K.K., Tomlinson, A., Foulks, G.N., Geerling, G., Pepose, J.S., Kosheleff, V., Porreco, A., Lemp, M.A.: An objective approach to dry eye disease severity. *Invest. Ophthalmol. Vis. Sci.* **51**(12), 6125–6130 (2010)
- [52] Dartt, D., Willcox, M.: Complexity of the tear film: importance in homeostasis

- and dysfunction during disease. *Exp. Eye Res.* **117**, 1–3 (2013)
- [53] Liu, H., Begley, C., Chen, M., Bradley, A., Bonanno, J., McNamara, N.A., Nelson, J.D., Simpson, T.: A link between tear instability and hyperosmolarity in dry eye. *Invest. Ophthalmol. Vis. Sci.* **50**(8), 3671–3679 (2009)
- [54] Luke, R.A., Braun, R.J., Driscoll, T.A., Begley, C.G., Awisi-Gyau, D.: Parameter Estimation for Evaporation-Driven Tear Film Thinning. *Bull. Math. Biol.* **82**(6), 71 (2020)
- [55] Pflugfelder, S.C.: Tear dysfunction and the cornea: LXVIII Edward Jackson memorial lecture. *Am. J. Ophthalmol.* **152**(6), 900–909 (2011)
- [56] Belmonte, C., Acosta, M.C., Merayo-Llodes, J., Gallar, J.: What causes eye pain? *Curr. Ophthalmol. Rep.* **3**(2), 111–121 (2015)
- [57] Nichols, J.J., Mitchell, G.L., King-Smith, P.E.: Thinning rate of the precorneal and prelens tear films. *Invest. Ophthalmol. Vis. Sci.* **46**(7), 2353–2361 (2005)
- [58] Hamano, H., Hori, M., Mitsunaga, S.: Measurement of evaporation rate of water from the precorneal tear film and contact lenses. *Contacto* **25**(2), 7–15 (1981)
- [59] Peng, C.-C., Cerretani, C., Li, Y., Bowers, S., Shahsavarani, S., Lin, M., Radke, C.: Flow evaporimeter to assess evaporative resistance of human tear-film lipid layer. *Ind. Eng. Chem. Res.* **53**(47), 18130–18139 (2014)
- [60] Dursch, T.J., Li, W., Taraz, B., Lin, M.C., Radke, C.J.: Tear-film evaporation rate from simultaneous ocular-surface temperature and tear-breakup area. *Optom. Vis. Sci.* **95**, 5–12 (2018)
- [61] Braun, R.J., Driscoll, T.A., Begley, C.G., King-Smith, P.E., Siddique, J.I.: On tear film breakup (TBU): Dynamics and imaging. *Math. Med. Biol.* **45**, 145–180 (2018)
- [62] Tiffany, J.M., Dart, J.K.G.: Normal and abnormal functions of meibomian secretion. *R. Soc. Med. Int. Congr. Symp.* **40**, 1061–4 (1981)
- [63] Purslow, C., Wolffsohn, J.S.: Ocular surface temperature: A review. *Eye Contact Lens* **31**, 117–123 (2005)
- [64] Tiffany, J.M.: Viscoelastic properties of human tears and polymer solutions. In: Sullivan, D.A. (ed.) *Lacrimal Gland, Tear Film, and Dry Eye Syndromes*, pp. 267–70. Plenum Press, New York (1994)
- [65] Pandit, J.C., Nagyová, B., Bron, A.J., Tiffany, J.M.: Physical properties of stimulated and unstimulated tears. *Exp. Eye Res.* **68**, 247–53 (1999)
- [66] Tiffany, J.M.: The viscosity of human tears. *Intl. Ophthalmol.* **15**, 371–376

(1991)

- [67] Jossic, L., Lefevre, P., Loubens, C., Magnin, A., Corre, C.: The fluid mechanics of shear-thinning tear substitutes. *J. Nonnewton. Fluid Mech.* **161**, 1–9 (2009)
- [68] Tiffany, J.M., Nagyová, B.: Components of tears responsible for surface tension. In: Sullivan, D.A., Dartt, D.A., Meneray, M.A. (eds.) *Lacrimal Gland, Tear Film, and Dry Eye Syndromes 2*, pp. 581–5. Plenum Press, New York (1998)
- [69] Tiffany, J.M.: The lipid secretion of the meibomian glands. *Adv. Lipid Res.* **22**, 1–62 (1987)
- [70] Leiske, D.L., Leiske, C.I., Leiske, D.R., Toney, M.F., Senchyna, M., Ketelson, H.A., Meadows, D.L., Fuller, G.G.: Temperature-induced transitions in the structure and interfacial rheology of human meibum. *Biophys. J.* **102**, 369–376 (2011)
- [71] Leiske, D.L., Miller, C.E., Rosenfeld, L., Cerretani, C., Ayzner, A., Lin, B., Meron, M., Senchyna, M., Ketelson, H.A., Meadows, D., Srinivasan, S., Jones, L., Radke, C.J., Toney, M.F., Fuller, G.G.: Molecular structure of interfacial human meibum films. *Langmuir* **28**, 11858–11865 (2012)
- [72] Rosenfeld, L., Cerretani, C., Leiske, D.L., Toney, M.F., Radke, C.J., Fuller, G.G.: Structural and rheological properties of meibomian lipid. *Invest. Ophthalmol. Vis. Sci.* **54**(4), 2720–2732 (2013)
- [73] Miller, D.: Measurement of the surface tension of tears. *Arch. Ophthalmol.* **82**, 368–71 (1969)
- [74] Nagyová, B., Tiffany, J.M.: Components of tears responsible for surface tension. *Curr. Eye Res.* **19**, 4–11 (1999)
- [75] Mudgil, P., Millar, T.J.: Adsorption of lysozyme to phospholipid and Meibomian lipid monolayer films. *Coll. Surf. B: Biointerfaces* **48**, 128–37 (2006)
- [76] Mudgil, P., Millar, T.J.: The effect of Meibomian lipids and tear proteins on evaporation rate under controlled in vitro conditions. *Exp. Eye Res.* **86**, 622–8 (2008)
- [77] Butovich, I.A.: Tear film lipids. *Experimental Eye Research* **117**, 4–27 (2013)
- [78] Rantamäki, A.H., Holopainen, J.M.: The Effect of Phospholipids on Tear Film Lipid Layer Surface Activity. *Invest. Ophthalmol. Vis. Sci.* **58**, 149–154 (2017)
- [79] Galor, A., Sanchez, V., Jensen, A., Burton, M., Maus, K., Stephenson, D., Chalfant, C., Mandal, N.: Meibum sphingolipid composition is altered in individuals with meibomian gland dysfunction—a side by side comparison of meibum and tear sphingolipids. *The Ocular Surface* **23**, 87–95 (2022)

- [80] Georgiev, G.A., Eftimov, P., Yokoi, N.: Structure-function relationship of tear film lipid layer: A contemporary perspective. *Exp. Eye Res.* **163**, 17–28 (2017)
- [81] Braun, R.J., Driscoll, T.A., Begley, C.G.: Mathematical models of the tear film. In: *Ocular Fluid Dynamics*, pp. 387–432. Springer, Berlin (2019)
- [82] Braun, R.J., Usha, R., McFadden, G.B., Driscoll, T.A., Cook, L.P., King-Smith, P.E.: Thin film dynamics on a prolate spheroid with application to the cornea. *J. Eng. Math.* **73**, 121–138 (2012)
- [83] Maki, K.L., Braun, R.J., Henshaw, W.D., King-Smith, P.E.: Tear film dynamics on an eye-shaped domain I: pressure boundary conditions. *Math. Med. Biol.* **27**, 227–254 (2010)
- [84] Maki, K.L., Braun, R.J., Ucciferro, P., Henshaw, W.D., King-Smith, P.E.: Tear film dynamics on an eye-shaped domain. Part 2. Flux boundary conditions. *J. Fluid Mech.* **647**, 361–390 (2010)
- [85] Li, L., Braun, R.J., Maki, K.L., Henshaw, W.D., King-Smith, P.E.: Tear film dynamics with evaporation, wetting and time-dependent flux boundary condition on an eye-shaped domain. *Phys. Fluids* **26**, 052101 (2014)
- [86] Li, L., Braun, R.J., Henshaw, W.D., King-Smith, P.E.: Computed tear film and osmolarity dynamics on an eye-shaped domain. *Math. Med. Biol.* **33**, 123–157 (2016)
- [87] Li, L., Braun, R.J., Henshaw, W.D., King-Smith, P.E.: Computed flow and fluorescence over the ocular surface. *Math. Med. Biol.* **35**, 51–85 (2018)
- [88] Driscoll, T.A., Braun, R.J., Brosch, J.K.: Simulation of parabolic flow on an eye-shaped domain with moving boundary. *J. Eng. Math.* **111**(1), 111–126 (2018)
- [89] Maki, K.L., Henshaw, W., McManus, A., Braun, R., Chapp, D., Driscoll, T.: A model for tear film dynamics during a realistic blink. *Modeling and Artificial Intelligence in Ophthalmology* **2**(3), 21–27 (2019)
- [90] Gaffney, E.A., Tiffany, J.M., Yokoi, N., Bron, A.J.: A mass and solute balance model for tear volume and osmolarity in the normal and the dry eye. *Prog. Retinal Eye Res.* **29**, 59–78 (2010)
- [91] Sharma, A., Tiwari, S., Khanna, R., Tiffany, J.M.: Hydrodynamics of Meniscus-induced Thinning of the Tear Film. In: Sullivan, D.A., Dartt, D.A., Meneray, M.A. (eds.) *Advances in Experimental Medicine and Biology. Lacrimal Gland, Tear Film, and Dry Eye Syndromes 2*, vol. 438, pp. 425–431. Springer, Berlin (1998)
- [92] Wong, H., Fatt, I., Radke, C.: Deposition and thinning of the human tear film.

- J. Colloid Interface Sci. **184**(1), 44–51 (1996)
- [93] Miller, K.L., Polse, K.A., Radke, C.J.: Black line formation and the “perched” human tear film. *Curr. Eye Res.* **25**, 155–62 (2002)
- [94] Braun, R.J., Fitt, A.D.: Modeling the drainage of the precorneal tear film after a blink. *Math. Med. Biol.* **20**, 1–28 (2003)
- [95] Li, L., Braun, R.J.: A model for the human tear film with heating from within the eye. *Phys. Fluids* **24**, 062103 (2012)
- [96] Jones, M.B., Please, C.P., McElwain, D.L.S., Fulford, G.R., Roberts, A.P., Collins, M.J.: Dynamics of tear film deposition and draining. *Math. Med. Biol.* **22**, 265–88 (2005)
- [97] Jones, M.B., McElwain, D.L.S., Fulford, G.R., Collins, M.J., Roberts, A.P.: The effect of the lipid layer on tear film behavior. *Bull. Math. Biol.* **68**, 1355–81 (2006)
- [98] Maki, K.L., Braun, R.J., Driscoll, T.A., King-Smith, P.E.: An overset grid method for the study of reflex tearing. *Math. Med. Biol.* **25**, 187–214 (2008)
- [99] Aydemir, E., Breward, C.J.W., Witelski, T.P.: The effect of polar lipids on tear film dynamics. *Bull. Math. Biol.* **73**, 1171–1201 (2010)
- [100] Bruna, M., Breward, C.J.W.: The influence of non-polar lipids on tear film dynamics. *J. Fluid Mech.* **746**, 565–605 (2014)
- [101] Allouche, M., Abderrahmane, H.A., Djouadi, S.M., Mansouri, K.: Influence of curvature on tear film dynamics. *Eur. J. Mech. B Fluids* **66**, 81–91 (2017)
- [102] Mehdaoui, H., Abderrahmane, H.A., Bouda, F.N., Koulali, A.: 2D numerical simulation of tear film dynamics: effects of shear-thinning properties. *Eur. J. Mech. B Fluids* **90**, 128–136 (2021)
- [103] Braun, R.J., King-Smith, P.E.: Model problems for the tear film in a blink cycle: Single equation models. *J. Fluid Mech.* **586**, 465–90 (2007)
- [104] Heryudono, A., Braun, R.J., Driscoll, T.A., Maki, K.L., Cook, L.P., King-Smith, P.E.: Single-equation models for the tear film in a blink cycle: realistic lid motion. *Math. Med. Biol. J. IMA* **24**(4), 347–377 (2007)
- [105] Zubkov, V.S., Breward, C.J.W., Gaffney, E.A.: Coupling fluid and solute dynamics within the ocular surface tear film: a modelling study of black line osmolarity. *Bull. Math. Biol.* **74**(9), 2062–2093 (2012)
- [106] Deng, Q., Braun, R.J., Driscoll, T.A.: Heat transfer and tear film dynamics over multiple blink cycles. *Phys. Fluids* **26**(7), 071901 (2014)

- [107] Deng, Q., Braun, R.J., Driscoll, T.A., King-Smith, P.E.: A model for the tear film and ocular surface temperature for partial blinks. *Interfacial Phenom. Heat Transf.* **1**(4) (2013)
- [108] Luke, R.A., Braun, R.J., Begley, C.G.: Mechanistic determination of tear film thinning via fitting simplified models to tear breakup. *Model. Artif. Int. Ophthalmol.* **3**, 71–100 (2021)
- [109] Driscoll, T.A., Braun, R.J., Luke, R.A., Sinopoli, D., Phatak, A., Dorsch, J., Begley, C.G., Awisi-Gyau, D.: Fitting ODE models of tear film breakup. *Model. Art. Int. Ophthalmol.* **5**(1), 1–36 (2023)
- [110] Zhong, L., Ketelaar, C.F., Braun, R.J., Begley, C.G., King-Smith, P.E.: Mathematical modeling of glob-driven tear film breakup. *Math. Med. Biol.*, 1–37 (2018)
- [111] Zhong, L., Braun, R.J., King-Smith, P.E., Begley, C.G.: Mathematical modeling of glob-driven tear film breakup. *J. Model. Ophthalmol.* **2**(1), 24–28 (2018)
- [112] Dey, M., Vivek, A.S., Dixit, H.N., Richhariya, A., Feng, J.J.: A model of tear-film breakup with continuous mucin concentration and viscosity profiles. *J. Fluid Mech.* **858**, 352–376 (2019)
- [113] Dey, M., Vivek, A.S., Dixit, H.N., Richhariya, A., Feng, J.J.: A model of tear-film breakup with continuous mucin concentration and viscosity profiles—Corrigendum. *J. Fluid Mech.* **889**, 1 (2020)
- [114] Choudhury, A., Dey, M., Dixit, H.N., Feng, J.J.: Tear-film breakup: The role of membrane-associated mucin polymers. *Phys. Rev. E* **103**, 013018 (2021)
- [115] Ji, H., Witelski, T.P.: Finite-time thin film rupture driven by modified evaporative loss. *Physica D: Nonlinear Phenomena* **342**, 1–15 (2017)
- [116] Ji, H., Witelski, T.P.: Steady states and dynamics of a thin-film-type equation with non-conserved mass. *Eur. J. Appl. Math.* **31**, 968–1001 (2020)
- [117] Shi, X., Rodríguez-Hakim, M., Shaqfeh, E.S.G., Fuller, G.G.: Instability and symmetry breaking in binary evaporating thin films over a solid spherical dome. *J. Fluid Mech.* **915**, 45 (2021)
- [118] Shi, X., Fuller, G.G., Shaqfeh, E.S.G.: Instability and symmetry breaking of surfactant films over an air bubble. *J. Fluid Mech.* **953**, 26 (2022)
- [119] Pucker, A., Haworth, K.: The presence and significance of polar meibum and tear lipids. *Ocul. Surf.* **13**(1), 26–42 (2015)
- [120] Butovich, I.A.: Meibomian glands, meibum, and meibogenesis. *Exp. Eye Res.* **163**, 2–16 (2017)

- [121] Georgiev, G.A., Borchman, D., Eftimov, P., Yokoi, N.: Lipid saturation and the rheology of human tear lipids. *Int. J. Molec. Sci.* **20**, 3431 (2019)
- [122] McCulley, J.P., Shine, W.: A compositional based model for the tear film lipid layer. *Tr. Am. Ophthalmol. Soc.* **XCIV**, 79–93 (1997)
- [123] Cerretani, C.F., Ho, N.H., Radke, C.: Water-evaporation reduction by duplex films: Application to the human tear film. *Adv. Colloid Interface Sci.* **197**, 33–57 (2013)
- [124] Sledge, S.M., Khimji, H., Borchman, D., Oliver, A.L., Michael, H., Dennis, E., Gerlach, D., Bhola, R., Stephen, E.: Evaporation and hydrocarbon chain conformation of surface lipid films. *Ocul. Surf.* **14**(4), 447–459 (2016)
- [125] Xu, X., Li, G., Zuo, Y.Y.: Effect of Model Tear Film Lipid Layer on Water Evaporation. *Invest. Ophthalmol. Vis. Sci.* **64**(1), 13 (2023)
- [126] King-Smith, P.E., Reuter, K.S., Braun, R.J., Nichols, J.J., Nichols, K.K.: Tear film breakup and structure studied by simultaneous video recording of fluorescence and tear film lipid layer, TFLL, images. *Invest. Ophthalmol. Vis. Sci.* **54**, 4900–4909 (2013)
- [127] Fenner, B.J., Tong, L.: More to Stable Tears Than Thickness of the Tear Film Lipid Layer. *Invest. Ophthalmol. Vis. Sci.* **56**(3), 1601–1601 (2015)
- [128] King-Smith, P.E., Braun, R.J.: Author Response: More to Stable Tears Than Thickness of the Lipid Layer. *Invest. Ophthalmol. Vis. Sci.* **56**(3), 1602–1602 (2015)
- [129] Wizert, A., Iskander, D., Cwiklik, L.: Organization of lipids in the tear film: A molecular-level view. *PLoS ONE* **9**, 92461 (2014)
- [130] Cwiklik, L.: Tear film lipid layer: A molecular level view. *Biochimica et Biophysica Acta* **1858**, 2421–2430 (2016)
- [131] Bland, H.C., Moilanen, J.A., Ekholm, F.S., Paananen, R.O.: Investigating the role of specific tear film lipids connected to dry eye syndrome: A study on o-acyl- ω -hydroxy fatty acids and diesters. *Langmuir* **35**(9), 3545–3552 (2019)
- [132] Viitaja, T., Moilanen, J., Svedström, K.J., Ekholm, F.S., Paananen, R.O.: Tear film lipid layer structure: Self-assembly of o-acyl- ω -hydroxy fatty acids and wax esters into evaporation-resistant monolayers. *Nano Letters* **21**(18), 7676–7683 (2021)
- [133] Paananen, R.O., Javanainen, M., Holopainen, J.M., Vattulainen, I.: Crystalline wax esters regulate the evaporation resistance of tear film lipid layers associated with dry eye syndrome. *J. Phys. Chem. Lett.* **10**(14), 3893–3898 (2019)

- [134] Butovich, I.A., Lu, H., McMahon, A., Ketelson, H., Senchyna, M., Meadows, D., Campbell, E., Molai, M., Linsenbardt, E.: Biophysical and morphological evaluation of human normal and dry eye meibum using hot stage polarized light microscopy. *Invest. Ophthalmol. Vis. Sci.* **55**(1), 87–101 (2014)
- [135] Stapf, M.R., Braun, R.J., King-Smith, P.E.: Duplex tear film evaporation analysis. *Bull. Math. Biol.* **79**(12), 2814–2846 (2017)
- [136] Taranchuk, M.J., Braun, R.J.: On the effect of liquid crystal orientation in the lipid layer on tear film thinning and breakup. *ArXiv* (2404.13225 [physics.flu-dyn]) (2024)
- [137] Matar, O.K., Craster, R.V., Warner, M.R.E.: Surfactant transport on highly viscous surface films. *J. Fluid Mech.* **466**, 85–111 (2002)
- [138] Cummings, L.J., Low, J., Myers, T.G.: Extensional flow of nematic liquid crystal with an applied electric field. *Eur. J. Appl. Math.* **25**(4), 397–423 (2014)
- [139] Taranchuk, M.J., Cummings, L.J., Driscoll, T.A., Braun, R.J.: Extensional flow of a free film of nematic liquid crystal with moderate elasticity. *Phys. Fluids* **35**(6) (2023)
- [140] King-Smith, P.E., Hinel, E.A., Nichols, J.J.: Application of a novel interferometric method to investigate the relation between lipid layer thickness and tear film thinning. *Invest. Ophthalmol. Vis. Sci.* **51**, 2418–2423 (2010)
- [141] King-Smith, P.E., Nichols, J.J., Braun, R.J., Nichols, K.K.: High resolution microscopy of the lipid layer of the tear film. *Ocul. Surf.* **9**(4), 197–211 (2011)
- [142] Goto, E., Tseng, S.C.G.: Kinetic analysis of tear interference images in aqueous tear deficiency dry eye before and after punctal occlusion. *Invest. Ophthalmol. Vis. Sci.* **44**, 1897–1905 (2003)
- [143] King-Smith, E., Fink, B., Hill, R., Koelling, K., Tiffany, J.: The thickness of the tear film. *Curr. Eye Res.* **29**(4-5), 357–368 (2004)
- [144] Stewart, I.W.: *The Static and Dynamic Continuum Theory of Liquid Crystals: a Mathematical Introduction*. CRC Press, Boca Raton, FL (2019)
- [145] Weast, R.C., Astle, M.J.: *CRC Handbook of Chemistry and Physics: A Ready-reference Book of Chemical and Physical Data*. CRC Press, Boca Raton, FL (1978)
- [146] Tiffany, J.M.: The lipid secretion of the meibomian glands. *Adv. Lipid Res.* **22**, 1–62 (1987)
- [147] Nagyova, B., Tiffany, J.M.: Components responsible for the surface tension of human tears. *Curr. Eye Res.* **19**(1), 4–11 (1999)

- [148] Riquelme, R., Lira, I., Pérez-López, C., Rayas, J.A., Rodríguez-Vera, R.: Interferometric measurement of a diffusion coefficient: comparison of two methods and uncertainty analysis. *J. Phys. D: Appl. Phys.* **40**(9), 2769 (2007)
- [149] Braun, R.J., Naire, S., Snow, S.A.: Limiting cases of gravitational drainage of a vertical free film for evaluating surfactants. *SIAM J. Appl. Math.* **61**, 889–913 (2000)
- [150] Stebe, K.J., Maldarelli, C.: Remobilizing surfactant retarded fluid particle interfaces: II. controlling the surface mobility at interfaces of solutions containing surface active components. *J. Coll. Interface Sci.* **163**(1), 177–189 (1994)
- [151] Paananen, R.O., Viitaja, T., Olzyska, A., Ekholm, F.S., Moilanen, J., Cwiklik, L.: Interactions of polar lipids with cholesteryl ester multilayers elucidate tear film lipid layer structure. *Ocul. Surf.* **18**, 545–553 (2020)
- [152] Stone, H.: A simple derivation of the time-dependent convective-diffusion equation for surfactant transport along a deforming interface. *Phys. Fluids A* **2**, 111–112 (1990)

